AGU PUBLICATIONS

Water Resources Research

RESEARCH ARTICLE
10.1002/2013WR014909

Key Points:
- Model transient streaming potentials in couple unsaturated-saturated zone flow
- Comparison of model predicted and measured responses
- Model used to estimate aquifer properties from transient SP data

Correspondence to:
B. Malama,
bnmalam@sandia.gov

Citation:
Malama, B. (2014), Theory of transient streaming potentials in coupled unconfined aquifer-unsaturated zone flow to a well, *Water Resour. Res.*, *50*, 2921–2945, doi:10.1002/2013WR014909.

Received 16 OCT 2013
Accepted 14 MAR 2014
Accepted article online 19 MAR 2014
Published online 2 APR 2014

Theory of transient streaming potentials in coupled unconfined aquifer-unsaturated zone flow to a well

Bwalya Malama[1]

[1]Performance Assessment Department, Sandia National Laboratories, Carlsbad, New Mexico, USA

Abstract A semianalytical solution is presented for transient streaming potentials associated with flow to a pumping well in an unconfined aquifer, taking into account the effect of flow in the unsaturated zone above the water table. Flow in the unsaturated zone is modeled with a linearized form of Richards' equation using an exponential model for soil moisture retention and unsaturated hydraulic conductivity. Archie's law is invoked for unsaturated electrical conductivity. The unsaturated electrokinetic coupling coefficient is modeled with a decaying exponential, where the maximum value is at and below the water table. The coupled flow and electrokinetic problem is solved using Laplace and Hankel transforms. The results of the model predicted behavior are presented and compared to that observed in laboratory simulations of pumping tests. The early time *polarity* reversal predicted the model is observable in the experiments. Other nonmonotonic streaming potential behaviors predicted by the model are also evident in experimental measurements. The model is used to estimate hydraulic parameters from SP data and these compare well to those obtained from drawdown data. For example, a hydraulic conductivity of 3.6×10^{-4} m/s is obtained from SP data compared to 3.4×10^{-4} m/s from drawdown data.

1. Introduction

Measurement of streaming potentials (SP) associated with groundwater flow has emerged as a viable hydrogeophysics tool for hydraulic characterization of the subsurface. SP signals are generated by fluid flow in the presence of an electric double layer (EDL) that develops at the water-mineral grain interface [e.g., *Ishido and Mizutani*, 1981; *Linde et al*., 2011; *Revil and Mahardika*, 2013, and references therein]. In its simplest form, the EDL comprises an immobile layer of ions attached to the mineral grain and a diffuse layer with excess ions that are dragged by pore water flow. This drag of excess diffuse layer ions constitutes a streaming current, which is responsible for the electric field that develops in the flow domain [*Chandler*, 1981; *Ishido and Mizutani*, 1981; *Sill*, 1983; *Titov et al*., 2002]. The SP method involves measurement of electric potentials associated with this electric field and using them to infer the behavior and properties of the hydraulic system.

Bogoslovsky and Ogilvy [1973] were among the first to measure SP during pumping tests with a view to characterizing the hydraulic system. Their data were later used by *Revil et al*. [2003] and *Darnet et al*. [2003] to estimate aquifer hydraulic conductivity and the extent of the cone of depression. Recently, *Rizzo et al*. [2004] measured the SP response associated with the recovery phase of a confined aquifer pumping test. They developed a model for steady state analysis and estimate hydraulic parameters from their SP data. Other attempts to estimate aquifer properties from SP data include *Sailhac and Marquis* [2001], *Suski et al*. [2004], *Titov et al*. [2002, 2005], and *Straface et al*. [2010]. *Maineult et al*. [2008] conducted periodic confined aquifer pumping tests and used the associated SP response to characterize the aquifer.

Malama et al. [2009b] recently developed a more complete semianalytical model for transient SP associated with flow to a well in a homogeneous confined aquifer. The model was used to estimate aquifer hydraulic parameters from the SP data of *Rizzo et al*. [2004]. The transient theory of SP was extended to unconfined aquifer flow by *Malama et al*. [2009a], who treated the water table as a material boundary, in the manner of *Neuman* [1972]. This approach neglects the effect of unsaturated zone flow on the pressure response of the aquifer. It is well documented in the hydrogeology literature, however, that this assumption leads to unusually low estimates of specific yield [*Nwankwor et al*., 1984; *Moench*, 1994, 1995; *Moench et al*., 2001; *Malama*, 2011]. This notwithstanding, the model of *Malama et al*. [2009a] was used to aquifer properties from SP data collected during pumping tests at the Boise Hydrogeophysical Research Site (BHRS).

Doussan et al. [2002] and *Linde et al*. [2011] have shown that the unsaturated zone plays an important role in the generation of SP signals. Their results imply that knowledge of the unsaturated electrokinetic coupling coefficient is essential to development of models incorporating unsaturated flow effects. Measurements of the electrokinetic coupling coefficient were carried in column experiments by *Guichet et al*. [2003]. *Revil and Cerepi* [2004] introduced the term relative coupling coefficient for unsaturated (two-phase) flow conditions. *Linde et al*. [2007] developed a model were the coupling coefficient varies roughly inversely as moisture saturation. The model has been used by *Revil et al*. [2007], *Mboh et al*. [2012], and *Jougnot and Linde* [2013] with reasonable success in modeling SP generation in the unsaturated zone. For some choices of unsaturated zone parameters, the model predicts a coupling coefficient that increases monotonically with increasing saturation. However, recent work by *Vinogradov and Jackson* [2011] give empirical evidence of a relative coupling coefficient that varies nonmonotonically with saturation. Thus, more general models that account surface electrical conductivity have thus been proposed by *Jackson* [2010] and *Jougnot et al*. [2012] to describe this nonmonotonic behavior. For sandy soils, however, where the surface conductivity may be neglected, experimental data indicate monotonic decay of the relative coupling coefficient with decreasing saturation [*Linde et al*., 2007; *Mboh et al*., 2012; *Jougnot and Linde*, 2013].

This work extends the development of *Malama et al*. [2009a] by accounting for flow in the unsaturated zone. *Revil et al*. [2008] presented similar modeling work where a numerical code was used to account for unsaturated flow effects during harmonic pumping tests. The present work is a development of a semianalytical solution that may be used to validate such numerical codes. The flow theory of *Mishra and Neuman* [2010], where a linearized form of Richards' equation is solved for unsaturated zone flow, is used as the basis for the SP problem formulation. The exponential model of *Gardner* [1958] is adopted for unsaturated zone constitutive relations. System hysteresis is ignored. For mathematical tractability, it is further assumed that surface conductivity is negligible and the coupling coefficient decays monotonically from the water table toward land surface.

In field conditions, SP signals associated with groundwater flow are usually small (a few to tens of millivolts) and vulnerable to corruption by noise. Hence, the solution developed in this work is first applied to transient SP data obtained in controlled laboratory simulations of unconfined aquifer pumping tests. Other attempts to study the physics of SP generation in low-noise lab-scale environments include the works of *Suski et al*. [2004], *Straface et al*. [2010, 2011], and *Malama* [2013]. In this work, we follow this pattern of laboratory experiments. In the following, we present (1) a statement of the SP problem and discussion of constitutive relations, (2) an outline of the solution, with details of the derivation supplied in Appendix B, (3) a discussion of model predicted behavior, (4) a description of laboratory experiments, (5) a parameter estimation exercise, where the model is fit to pumping phase SP data, and (6) concluding remarks.

2. Mathematical Formulation

The SP response to groundwater flow toward a fully penetrating pumping well in a homogeneous and radially infinite unconfined aquifer is considered here. The groundwater flow problem is assumed to be described by the model of *Mishra and Neuman* [2010] who included the effects of flow in the unsaturated zone using a linearized form of Richards' equation and the Gardner model to describe the unsaturated zone constitutive relations. The additional simplification of a line sink for the pumping well is also adopted here. The flow problem and the associated initial, boundary, and continuity conditions are given in the Appendix A. The derivation of the exact analytical solution in Laplace and Hankel transform space is also given in the Appendix A. The flow problem is solved in a slightly different manner from the approach of *Mishra and Neuman* [2010] who specify a homogeneous Neumann (no fluid flux) boundary condition at land surface. In this work, this condition is relaxed by only requiring that the hydraulic response in the unsaturated zone remains finite even as the thickness of the zone becomes very large. This assumption leads to a solution that is much simpler flow than that obtained by *Mishra and Neuman* [2010] but still correctly describes the characteristic hydraulic response of an unconfined aquifer to pumping.

2.1. The SP Problem

Whereas the flow problem is solved on a two-layered domain, consisting of the saturated and unsaturated zones, the SP problem is solved on a three-layered domain because an insulating boundary condition at

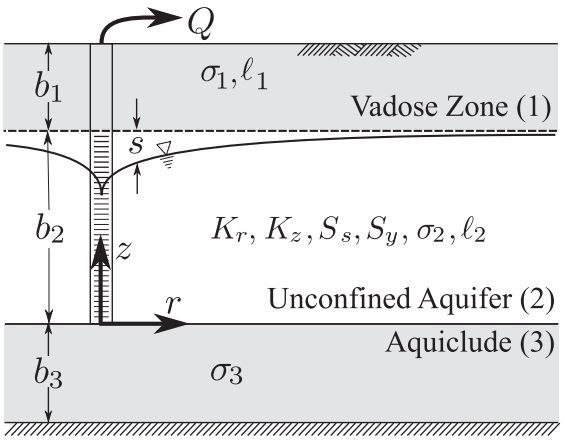

Figure 1. Schematic of the three-layer conceptual model used to develop the SP solution.

the base of the aquifer is not realistic. This is particularly the case when the aquifer is underlain with a highly electrically conductive but not hydraulically conductive clay layer. For cases where the aquifer is underlain with highly resistive bedrock, this more general conceptual model may still be used, with a vanishingly small electrical conductivity for the bedrock. The three-layered system comprises the unsaturated zone ($i=1$) above the water table, the saturated zone or unconfined aquifer ($i=2$), and the confining unit ($i=3$) below the aquifer. It is shown schematically in Figure 1.

The electric field in the *i*th layer is governed by [*Revil et al*., 2003]

$$\nabla \cdot \mathbf{j}_i = 0, \psi \tag{1}$$

where $\mathbf{j}_i$ is the electric current density (A/m^2). *Revil et al*. [2003, and references therein] have shown that

$$\mathbf{j}_i = \sigma_i \mathbf{E}_i + \mathbf{j}_{f,i}, \psi \tag{2}$$

where σ_i is the bulk medium electrical conductivity (S/m), $\mathbf{E}_i = -\nabla\phi_i$ is the electric field (V/m), $\phi_i = \varphi_i - \varphi_{i,0}$ is the electric potential change (V) from some initial state $\varphi_{i,0}$, and $\mathbf{j}_{f,i}$ is the electric current density due to fluid flow and is given by [e.g., *Sailhac and Marquis*, 2001; *Malama et al*., 2009b]

$$\mathbf{j}_{f,i} = \sigma C_{\ell,i} \mathbf{K}_i^{-1} \mathbf{q}_i, \psi \tag{3}$$

where $C_{\ell,i} = -\partial\phi_i / \partial h_i$ is the electrokinetic coupling coefficient (V/m), $\mathbf{K}_i$ is the hydraulic conductivity tensor, $\mathbf{q}_i = -\mathbf{K}_i \nabla h_i$ is the Darcy fluid flux (m/s), and h_i is hydraulic head (m). Note that φ_i is the potential difference between an observation point electrode and a reference electrode, and $\varphi_{i,0} = \varphi_i(t=0)$.

To solve the couple flow-SP problem, the following simplifying assumptions are made:

1. Aquifer is isotropic, homogeneous, radially infinite, and bounded above and below by horizontal boundaries,
2. Pumping well is a line sink (vanishingly small radius) and is fully penetrating,
3. No flow at land surface (no evaporation/precipitation) and in the unit below the aquifer,
4. Quasi-static limit is satisfied at all times,
5. Initial potential is zero everywhere in the domain relative to some reference,
6. Homogeneous and isotropic electrical conductivity and coupling coefficient,
7. Monotonically decaying unsaturated zone coupling coefficient, and
8. Negligible surface electrical conductivity.

With these assumptions, substituting equations (2) and (3) and Darcy's law into (1) for the unsaturated zone yields

$$\nabla \cdot [\sigma_1(z) \nabla \phi_1(r,z,t)] = \nabla \cdot [\sigma_1(z) C_{\ell,1}(z) \nabla s_1(r,z,t)], \psi \tag{4}$$

where (r,z,t) are the space-time coordinates, ϕ_1 and s_1 are the changes in the unsaturated zone streaming and matric (suction) potentials, respectively, due pumping in the saturated zone, and σ_1 and $C_{\ell,1}$ are the unsaturated zone electrical conductivity and electrokinetic coupling coefficient, respectively. It is assumed

here that the parameters σ_1 and $C_{\ell,1}$ are functions of z only. This is a consequence of the linearization by *Tartakovsky and Neuman* [2007] of Richards' equation adopted by *Mishra and Neuman* [2010] to solve the flow problem, and is invoked here to solve the SP problem. Dividing throughout by σ_1 and applying the chain rule, it can be shown that equation (4) may be rewritten as

$$\nabla^2\phi_1 + \frac{\partial \ln(\sigma_1)}{\partial z}\frac{\partial \phi_1}{\partial z} = C_{\ell,1}\left[\nabla^2 s_1 + \frac{\partial \ln(\ell_h)}{\partial z}\frac{\partial s_1}{\partial z}\right], \psi \tag{5}$$

where $\ell_h = \sigma_1 C_{\ell,1}$. The right-hand side of this equation is defined by the flow solution in the unsaturated zone. Equation (5) is solved subject to the initial condition

$$\phi_1(r, z, 0) = 0, \psi \tag{6}$$

and the far-field homogeneous Dirichlet boundary condition

$$\lim_{r\to\infty\leftarrow} \phi_1(r, z, t) = 0, \psi \tag{7}$$

which follow directly from the definition of ϕ_i and implies no change from the initial value at $r = \infty$. The homogeneous Neumann boundary condition

$$\lim_{r\to 0} r\frac{\partial \phi_1}{\partial r} = 0, \psi \tag{8}$$

is applied along pumping well axis, and is simply a symmetry condition. Further, the solution satisfies $|\phi_1| < \psi\infty$ even as $z = b_1 + b_2 \to \infty$. This implies that ϕ_1 remains finite even as the thickness of the unsaturated zone becomes very large. Here b_1 and b_2 are the initial unsaturated and saturated zone thicknesses.

Similarly, the governing equation for the SP response in the saturated zone is given by

$$\nabla^2\phi_2 = C_{\ell,2}\nabla^2 s_2, \psi \tag{9}$$

where $C_{\ell,2}$ is the aquifer electrokinetic coupling coefficient, and ϕ_2 and s_2 are the SP and drawdown responses of the aquifer to pumping. Here $s_2 = h_2(r, z, t) - h_2(r, z, 0)$, where h_2 is aquifer hydraulic head. Equation (9) is solved subject to the initial condition

$$\phi_2(r, z, 0) = 0, \psi \tag{10}$$

the far-field homogeneous Dirichlet boundary condition

$$\lim_{r\to\infty\leftarrow} \phi_2(r, z, t) = 0, \psi \tag{11}$$

and the line-sink pumping well boundary condition

$$\lim_{r\to 0} r\frac{\partial \phi_2}{\partial r} = -\frac{Q}{2\pi b_2 K_r} C_{\ell,2}, \psi \tag{12}$$

where Q is the pumping rate, b_2 is the initial saturated thickness of the aquifer, and K_r is the radial hydraulic conductivity of the aquifer.

For the confining unit below the aquifer, the governing equation for the SP response, ϕ_3, is given by the Laplace equation, viz,

$$\nabla^2\phi_3 = 0, \psi \tag{13}$$

since no fluid flow is assumed to occur in this layer (i.e., negligible leakage). The initial and far-field boundary conditions are given by

$$\phi_3(r,z,0)=\lim_{r\to\infty}\phi_3(r,z,t)=0. \tag{14}$$

Since there is no pumping in this layer, the homogeneous Neumann boundary condition

$$\lim_{r\to 0} r\frac{\partial\phi_3}{\partial r}=0, \tag{15}$$

is imposed along the pumping well axis. Additionally, the finiteness constraint, $|\phi_3|<\infty$ even as $z=-b_3\to-\infty$, is imposed on the SP response in the confining layer.

The initial and boundary conditions given above are necessary but not sufficient to solve the SP problem. To complete the statement of the problem, potential and potential gradient continuity conditions are imposed at the water table,

$$\phi_2|_{z=b_2}=\phi_1|_{z=b_2}, \tag{16}$$

$$\sigma_2\frac{\partial\phi_2}{\partial z}\Big|_{z=b_2}=\sigma_1\frac{\partial\phi_1}{\partial z}\Big|_{z=b_2}, \tag{17}$$

and at the base of the aquifer,

$$\phi_2|_{z=0}=\phi_3|_{z=0}, \tag{18}$$

$$\sigma_2\frac{\partial\phi_2}{\partial z}\Big|_{z=0}=\sigma_3\frac{\partial\phi_3}{\partial z}\Big|_{z=0}, \tag{19}$$

where σ_3 is the electrical conductivity of the confining unit. The next step is to specify the functional forms of $\sigma_1(z)$, $C_{\ell,r}(z)$, and the unsaturated hydraulic parameters. This is discussed in the following sections.

2.2. Unsaturated Zone Constitutive Relations

The constitutive relations used in this work follow the assumption of *Mishra and Neuman* [2010] that the moisture retention curve and the unsaturated hydraulic conductivity are described by the exponential model of *Gardner* [1958], viz,

$$S_w(\psi)=e^{a_c(\psi-\psi_a)}, \tag{20}$$

and

$$k_r(\psi)=e^{a_k(\psi-\psi_k)}, \tag{21}$$

where S_w is the saturation, k_r is the relative hydraulic conductivity, $a_c>0$ and $a_k>0$ are empirical constants, ψ is matric potential (suction head), ψ_a is the air entry (bubbling) pressure head, and ψ_k is the pressure head at which $k_r\approx 1$. For the flow problem, water saturation, S_w, is defined as

$$S_w(\psi)=\frac{\theta(\psi)-\theta_R}{\theta_{\text{sat}}-\theta_R}, \tag{22}$$

where $\theta(\psi)$ is volumetric soil moisture content expressed as a function of matric potential, ψ, and θ_R and θ_{sat} are residual and saturated moisture content, respectively. Using the linearization of *Tartakovsky and Neuman* [2007], i.e., $\psi\approx b_2+\psi_a-z$, it follows that

$$S_w(\psi)\approx e^{-a_c(z-b_2)}, \tag{23}$$

and

$$k_r(\psi)\approx e^{-a_k(\psi_k-\psi_a+z-b_2)}. \tag{24}$$

Equations (23) and (24) form the basis of the constitutive relations for unsaturated electrical conductivity and electrokinetic coupling coefficient presented below.

2.2.1. Electrical Conductivity

Assuming negligible surface conductivity, unsaturated zone electrical conductivity, σ_1, is given by Archie's law as [*Friedman*, 2005; *Revil et al*., 2007]

$$\sigma_1 = \sigma_w n^m \tilde{S}_w^d(\psi) = \sigma_{\text{sat}}\, \sigma_r(\psi), \psi \tag{25}$$

where σ_w is pore water electrical conductivity, n is porosity, m is Archie's cementation exponent, $\tilde{S}_w = \theta(\psi)/\theta_{\text{sat}}$, $\sigma_{\text{sat}} = \sigma_w n^m$, $\sigma_r(\psi) = \tilde{S}_w^d(\psi)$ is the relative electrical conductivity (unsaturated electrical conductivity normalized by that at saturation), and d is Archie's second exponent. Hence, using the linearization of *Tartakovsky and Neuman* [2007], it follows that

$$\sigma_r(\psi) \approx\ e^{-d a_c (z - b_2)}, \psi \tag{26}$$

The electrical conductivity at saturation is identical to that of the unconfined aquifer $(\sigma_1|_{z=b_2} = \sigma_{\text{sat}} = \sigma_2)$.

2.2.2. Electrokinetic Coupling Coefficient

The electrokinetic coupling coefficient for unsaturated media can be written as

$$C_{\ell,1} = C_{\ell,\text{sat}}\, C_{\ell,r}(\psi), \psi \tag{27}$$

where $C_{\ell,\text{sat}}$ is the coupling coefficient at saturation, which equals that of the aquifer, and $C_{\ell,r}$ is the relative coupling coefficient. It has been shown by *Revil et al*. [2007] and *Jackson* [2010] that $C_{\ell,r}$ is given by

$$C_{\ell,r}(\psi) = \frac{k_r(\psi)_{\leftarrow}}{\sigma_r(\psi)\tilde{S}_w(\psi)_{\leftarrow}} = k_r(\psi)\tilde{S}_w^{-(d+1)_{\leftarrow}}(\psi), \psi \tag{28}$$

which may be linearized as

$$C_{\ell,r}(\psi) \approx\ e^{a_c(\psi_a - \psi_k) + a_c d(z - b_2)}, \psi \tag{29}$$

using the approach of *Tartakovsky and Neuman* [2007] and the assumption that $a_k = a_c$. This function grows with vertical position above the water table (i.e., with $z - b_2$) for $d > 0$, which is at variance with published measurements. Empirical evidence [*Guichet et al*., 2003; *Revil et al*., 2004, 2007; *Mboh et al*., 2012] shows that $C_{\ell,r}$ decreases with decreasing soil moisture content, and consequently, with increasing vertical position above the water table. Hence, we propose using the decaying exponential function

$$\ell_\psi = \sigma_r C_{\ell,r} = e^{-a_\ell (z - b_2)}, \psi \tag{30}$$

for the relative electrokinetic coupling coefficient, where the constant parameter a_ℓ is a measure of the decay rate of $C_{\ell,r}$ with vertical position above the water table.

3. Governing Equations in Dimensionless Form

The governing equation for SP for the three-layer system can be rewritten in dimensionless form as

$$\nabla_D^2 \phi_{D,i} - \epsilon_i \beta_0 d \frac{\partial \phi_{D,i}}{\partial z_D} = C_{\ell,r} F_i(r_D, z_D, t_D) \quad \forall i = \{1, 2, 3\}, \psi \tag{31}$$

where $r_D = r/b_2$, $z_D = z/b_2$, $\phi_{D,1} = \phi_1/\Phi_c$, $\Phi_c = H_c C_{\ell,2}$, $H_c = Q/(4\pi b_2 K_r)$, $\beta_0 = a_c b_2$, $\varepsilon_1 = 1$, $\varepsilon_2 = \varepsilon_3 = 0$, $C_{\ell,r} = 1$ for $i = 2, 3$, and

$$F_i(r_D, z_D, t_D) = \nabla_D^2 s_{D,i} - \varepsilon_i \beta_1 \frac{\partial s_{D,i}}{\partial z_D}, \psi \tag{32}$$

with $\beta_1 = -\partial \ln(\ell_\psi)/\partial z_D = a_\ell b_2 = \text{constant}$, given the definition of ℓ_ψ in equation (30). Given that there is no flow in the confining unit, $F_3(r_D, z_D, t_D) \equiv 0$. The initial condition and far-field boundary condition become

Table 1. Dimensionless Variables and Parameters ($i = 1,2,3$)

$s_{D,i}=s_i/H_c$
$\phi_{D,i}=\phi_i/\Phi_c$
$r_D=r/b_2$
$z_D=z/b_2$
$t_D=\alpha_{r,2}t/b_2^2$
$b_{D,i}=b_i/b_2$
$\beta_0=a_c b_2=a_k b_2$
$\beta_1=a_\ell b_2=(1+\delta)\beta_0$
$\kappa=K_z/K_r$
$\sigma_{D,i}=\sigma_i/\sigma_2$
$\vartheta=(\beta_0 S_y/S_s)e^{-\beta_0(\psi_{D,a}-\psi_{D,k})}$
$\psi_{D,a}=\psi_a/b_2$
$\psi_{D,k}=\psi_k/b_2$

$$\phi_{D,i}(r_D,z_D,0)=\lim_{r_D\to\infty\leftarrow}\phi_{D,i}(r_D,z_D,t_D)=0,\psi \tag{33}$$

for $i=1, 2, 3$. It can be shown [*Malama et al.*, 2009b, 2009a] that the boundary conditions at $r_D=0$ can be written as

$$\lim_{r_D\to 0} r_D\frac{\partial\phi_{D,i}}{\partial r_D}=\begin{cases}0 & i=1,3\\ -2 & i=2.\psi\end{cases} \tag{34}$$

The continuity conditions at the water table have the form

$$\phi_{D,2}|_{z_D=1}=\phi_{D,1}|_{z_D=1},\psi \tag{35}$$

and

$$\frac{\partial\phi_{D,2}}{\partial z_D}\Big|_{z_D=1}=\frac{\partial\phi_{D,1}}{\partial z_D}\Big|_{z_D=1},\psi \tag{36}$$

given that the water table is always at saturation, in which case $\sigma_1=\sigma_{sat}=\sigma_2$. Continuity conditions at the aquifer base are

$$\phi_{D,2}|_{z_D=0}=\phi_{D,3}|_{z_D=0},\psi \tag{37}$$

$$\frac{\partial\phi_{D,2}}{\partial z_D}\Big|_{z_D=0}=\sigma_{D,3}\frac{\partial\phi_{D,3}}{\partial z_D}\Big|_{z_D=0},\psi \tag{38}$$

where $\sigma_{D,3}=\sigma_3/\sigma_2$. To complete the definition of the problem, the finiteness condition is imposed at land surface and at the base of the confining unit, viz,

$$|\phi_{D,1}|<\infty,\psi \tag{39}$$

even as $z_D=1+b_{D,1}\to\infty$, and

$$|\phi_{D,3}|<\infty,\psi \tag{40}$$

even as $z_D=-b_{D,1}\to\leftarrow\infty$, where $b_{D,1}=b_1/b_2$ and $b_{D,3}=b_3/b_2$. A complete list of the dimensionless variables and parameters is given in Table 1.

The parameter $\beta_1=a_\ell b_2$ follows from equation (30), which was introduced to ensure $C_{\ell,r}$ decays with decreasing moisture content upward from the water table. It captures the dependence of the unsaturated zone electrokinetic coupling coefficient, $C_{\ell,r}$ on vertical position (or moisture content) relative to the water table. Physically permissible values of β_1, for which the function $C_{\ell,r}$ decays upward from the water table, satisfy the condition $\beta_1\geq\beta_0 d$, where d is Archie's second exponent. Hence, to ensure that this condition is always satisfied we set $\beta_1=(1+\delta)\beta_0 d$, where $\delta\geq 0$ is a (dimensionless) measure of how much larger β_1 is than $\beta_0 d$.

4. Analytical Solution

The dimensionless SP governing equations outlined above are solved using Laplace and Hankel transforms (see Appendix B for derivation) yielding the solution

$$\bar\phi^*_{D,i}=\begin{cases}\bar\phi^{*(0)}_{D,1}(a,z_D,p)+\bar\phi^*_{D,p}(a,z_D,p)\leftarrow & \forall z_D>\psi1\\ \bar\phi^{*(0)}_{D,2}(a,z_D,p)+\bar s^*_{D,2}(a,z_D,p) & \forall z_D\in[0,1]\\ \bar\phi^*_{D,2}|_{z_D=0}e^{az_D} & \forall z_D<\psi0,\psi\end{cases} \tag{41}$$

where p and a are Laplace and Hankel transform parameters, respectively,

$$\phi_{D,1}^{(0)\leftarrow}(a,z_D,p)=\left[\phi_{D,2}^{(0)\leftarrow}+(1-\chi)s_{D,1}\right]\Big|_{z_D=1}e^{-\hat{u}(z_D-1)},\psi \tag{42}$$

$$\phi_{D,p}(a,z_D,p)=C_{\ell,r}(z_D)\chi(a,p)s_{D,1}(a,z_D,p),\psi \tag{43}$$

$$\phi_{D,2}^{(0)\leftarrow}(a,z_D,p)=\frac{1}{\Delta_1}[Z_1w_1(a,z_D)+Z_2w_2(a,z_D)],\psi \tag{44}$$

$$w_1(a,z_D)=\sigma_{D,3}\sinh(az_D)+\cosh(az_D),\psi \tag{45}$$

$$w_2(a,z_D)=\hat{u}\sinh[a(z_D-1)]-a\cosh[a(z_D-1)],\psi \tag{46}$$

$$Z_1=-[(\hat{u}+u)(1-\chi)+\beta_0 d\chi]s_{D,1}|_{z_D=1},\psi \tag{47}$$

$$Z_2=\sigma_{D,3}s_{D,2}|_{z_D=0},\psi \tag{48}$$

$$C_{\ell,r}=e^{-\delta\beta_0 d(z_D-1)},\psi \tag{49}$$

$$\chi(a,p)=\frac{u^2-\beta_1 u-a^2}{(u-\delta\beta_0 d)(u-\beta_1)-a^2},\psi \tag{50}$$

$u=u_0(1-v)$, $u_0=\beta_0/2$, $v^2=1+(\eta_1/u_0)^2$, $\hat{u}=u_0 d(\hat{v}-1)$, $\hat{v}^2=1+[a/(u_0 d)]^2$, $\eta^2=(p+a^2)/\kappa$, $\eta_1^2=(p\vartheta+a^2)/\kappa$, and

$$\Delta_1=|(\hat{u}\sigma_{D,3}+a)\sinh(a)+(a\sigma_{D,3}+\hat{u})\cosh(a)|.\psi \tag{51}$$

This solution can be used to analyze transient SP data collected at the land surface, in the unsaturated zone, or at depth in the unconfined aquifer.

The Laplace transforms are inverted numerically using the method of *de Hoog et al*. [1982]. Hankel transforms are also inverted numerically in the manner proposed by *Wieder* [1999] whereby the infinite integral is split into a series of finite integrals between zeros of the J_0 Bessel function, the summation of which is then accelerated using Euler's transformation [*Abramowitz and Stegun*, 1972]. The integration between zeros of the J_0 Bessel function is accomplished using adaptive Gauss-Kronrod quadrature as implemented in MATLAB [*Shampine*, 2008]. The inverse Hankel transform is computed first, after which the algorithm of *de Hoog et al*. [1982] is used to invert the Laplace transform.

5. Model Predicted SP Behavior

This section considers the effects of pertinent dimensionless parameters on the temporal behavior of the SP response predicted by the model presented above. The theoretical response, $\phi_{D,i}$, is plotted against dimensionless time, $t_D/r_D^2=\alpha t/r^2$ on semilog scale. The results discussed here, unless indicated otherwise, were computed with the dimensionless parameter values of $\kappa=1$, $S=2\times10^{-5}$, $\vartheta=1.5\times10^4$, $\beta_0=1$, $\psi_{D,a}-\psi_{D,k}=2.5\times10^{-4}$, $\sigma_{D,3}=10^3$, $d=2.7$, and $r_D=0.25$.

5.1. Unsaturated Zone Response

Typical SP responses predicted in the unsaturated zone by this model are shown in Figures 2 and 3. The results shown in Figure 2 were computed at land surface ($z_D=1+b_{D,1}$). Recall that $\phi_{D,1}=\phi_{D,1}^{(0)}+\phi_{D,p}$. The homogeneous solution may be rewritten as

$$\phi_{D,1}^{(0)\leftarrow}=\sum_{n=1}^{3}\phi_{D,1}^{(n)\leftarrow},\psi \tag{52}$$

where $\phi_{D,1}^{(n)\leftarrow}=f_n e^{-\hat{u}(z_D-1)}$,

$$f_1(a,p)=1-\frac{\hat{u}+u}{\Delta_1}w_1(a,1)\leftarrow s_{D,2}|_{z_D=1},$$

$$f_2(a,p)=-\chi\left[f_1+\frac{\beta_0 d}{\Delta_1}w_1(a,1)s_{D,2}|_{z_D=1}\right],$$

and

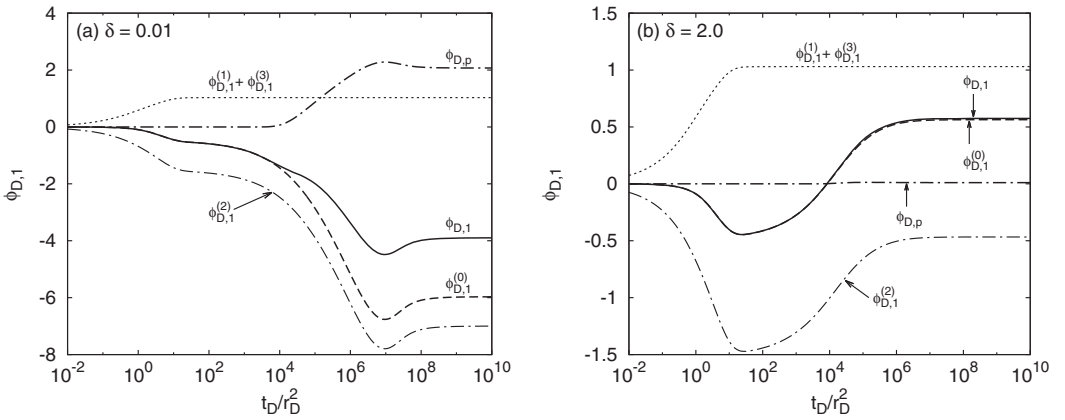

Figure 2. Model predicted SP response (ϕ_1) at land surface for (a) δ=0.01 and (b) δ=2, where $\delta=\beta_1/(\beta_0 d)-1$. Relative contributions of $\phi_{D,1}^{(0)}$ and $\phi_{D,p}$ to the total response, $\phi_{D,1}$, are included.

$$f_3(a,p)=-\frac{a\sigma_{D,3}}{\Delta_1}s_{D,2}|_{z_D=0}.\psi$$

The functions f_1 and f_2 account for the effects of unsaturated zone flow and water table movement and f_3 is strongly related to the boundary condition at the base of the aquifer. Further, f_2 accounts for the variation of the relative coupling coefficient with matric potential (or with z_D).

Strong unsaturated zone electrokinetic coupling is associated with a strongly negative model predicted response, whereas very weak coupling yields positive signals. This is due to the negative (inverse) correlation between hydraulic head and SP. The relative contributions of the homogeneous $(\phi_{D,1}^{(0)})$ and particular $(\phi_{D,p})$ solutions to the total unsaturated zone response are also shown in Figure 2. The function $\phi_{D,p}$ is the contribution of the source term associated with generation of streaming current by fluid drainage in the unsaturated zone. It diminishes in significance and becomes vanishingly small as δ increases due to rapid decay of relative coupling coefficient from the water table to land surface. In the example shown in Figure 2, the contribution of $\phi_{D,p}$ to the total response is significant in (a) where δ=0.01 but is negligibly small in (b) where δ=2. The results indicate that for $\delta > 1$, the contribution of fluid flow in the unsaturated zone to the SP response may be neglected and $\phi_{D,1} \approx \phi_{D,1}^{(0)}$. The parameter δ provides a measure of the difference between the rate of decay of soil moisture and the coupling coefficient with vertical displacement above the water table. For $\delta \ll 1.0$, the coupling coefficient decays at roughly the same rate as soil moisture with displacement from the water table to land surface.

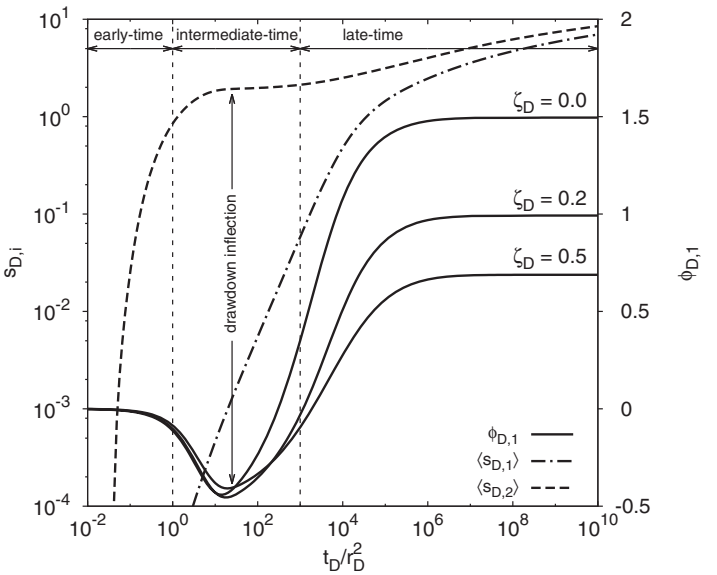

Figure 3. Model predicted SP response at different vertical positions, ζ_D, relative to the water table. The depth average unsaturated $(\langle s_{D,1}\rangle)$ and saturated $(\langle s_{D,2}\rangle)$ zone drawdown responses are included for comparison.

Figure 2 also includes plots of the functions $\phi_{D,1}^{(1)}+\phi_{D,1}^{(3)}$ and $\phi_{D,1}^{(2)}$ for the two different values of δ. The contribution of $\phi_{D,1}^{(1)}+\phi_{D,1}^{(3)}$ is invariant with δ because it is simply due to electrical conduction through the unsaturated zone. The contribution of $\phi_{D,1}^{(2)}$ diminishes due to

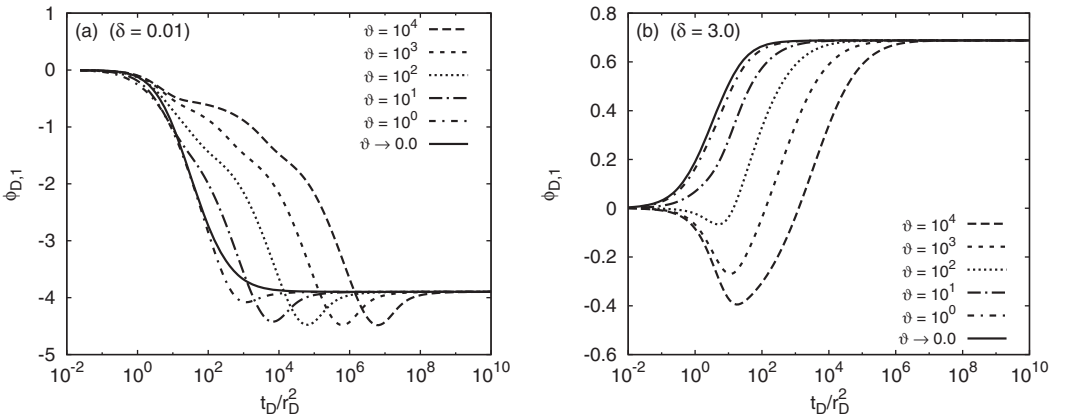

Figure 4. Temporal variation of model predicted unsaturated zone SP for (a) δ=0.01 and (b) δ=3 for different values of the dimensionless parameter ϑ.

decreased electrokinetic coupling. The competing effects of $\phi_{D,1}^{(1)\leftarrow}+\phi_{D,1}^{(3)\leftarrow}$ and $\phi_{D,1}^{(2)}$ explain the apparent increase in the model predicted SP signal with weakening electrokinetic coupling in the unsaturated zone; as $\phi_{D,1}^{(2)\leftarrow}$ approaches 0, the homogeneous response, $\phi_{D,1}^{(0)\leftarrow}$, approaches $\phi_{D,1}^{(1)\leftarrow}+\phi_{D,1}^{(3)\leftarrow}$.

Figure 3 shows the temporal variation of unsaturated zone SP response with vertical position $\zeta_D=z_D-1$ relative to the water table. Plots of vertically averaged unsaturated and saturated zone drawdown responses, $\langle s_{D,1}\rangle$ and $\langle s_{D,2}\rangle$, respectively, are included for comparison. Saturated zone drawdown responses associated with unconfined aquifer pumping tests are known to exhibit three temporal phases, namely early time, intermediate-time, and late-time responses. The early time response is attributed to instantaneous water release from elastic storage, whereas the intermediate-time response includes the effects of water release from water table displacement and unsaturated zone drainage. At late time, the aquifer is in the pseudo-static flow regime where the saturated and unsaturated zones act as a single saturated continuum.

The three phases discussed above are not observed at or above the water table for the hydraulic response. However, they are predicted by the model for the SP response throughout the unsaturated zone (from the water table, $\zeta_D=0$ to land surface). This is clearly evident in Figure 3. The early time response is attributed to charge release associated with the corresponding water release from elastic storage. A combination of charge release from elastic storage and charge influx into the saturated zone due to water table decline and drainage from the unsaturated zone leads to the intermediate-time and late-time responses. This implies that a characteristic unconfined SP response may be measurable in the unsaturated zone even when there is no detectable hydraulic response there.

For the unconfined aquifer flow problem, it is important to examine the effect of the two water storage mechanisms controlled by specific yield (S_y) and storativity ($S=b_2S_s$, S_s is specific storage) on system behavior. The model predicted transient streaming and matric potential responses at land surface for different values of the dimensionless storage parameter ϑ, defined as

$$\vartheta=\frac{\beta_0 S_y}{S}e^{-\beta_0(\psi_{D,a}-\psi_{D,k})},\psi \tag{53}$$

are shown in Figures 4a and 4b, respectively. The plots were generated with the parameters listed above except for $\beta_1=40$. The parameter ϑ is a measure of the relative contributions of water from gravity drainage of the unsaturated zone and the initially saturated pore space due to water table decline $(\beta_0 S_y e^{-\beta_0(\psi_{D,a}-\psi_{D,k})})$ versus water release from elastic storage as given by the storativity S. The results were obtained by varying S_y with β_0 and S fixed at 1 and 2×10^{-5}, respectively. They indicate significant sensitivity of the SP response to specific yield. This implies that measured SP responses can be used to estimate this parameter.

The predicted responses shown in Figure 4 vary from monotonic growth with time (small ϑ) to nonmonotonic responses that exhibit three distinct phases, namely, an early time phase where the SP decrease from zero to some minimum, an intermediate-time growth phase where the response increases from the

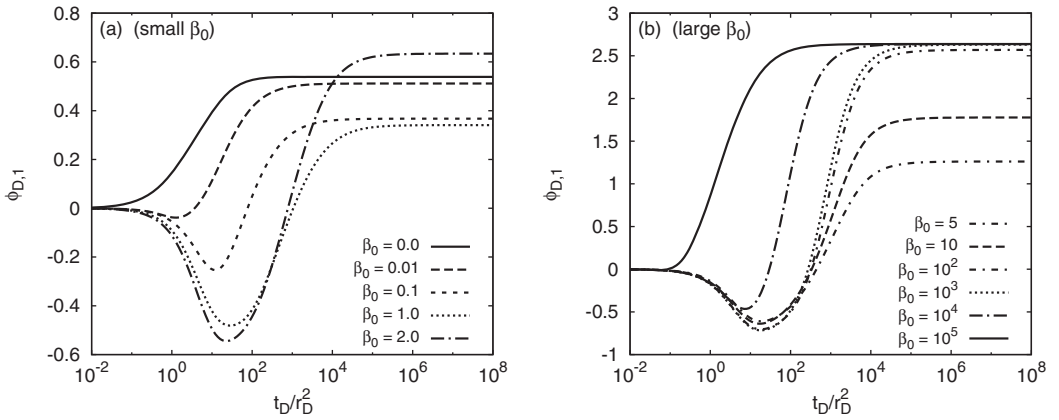

Figure 5. Temporal variation of model predicted unsaturated zone SP for different values of the dimensionless parameter β_0.

minimum attained in the early time phase, and a late-time steady state. The negative early time phase is due to water release from water table decline and the resultant flow in the unsaturated zone. Pumping removes charge from the system through the prescribed pumping well boundary condition, whereas flow from water table decline and unsaturated zone flow replenishes system charge. At early time outflow of system charge with water released from elastic storage far exceeds replenishment from water table decline and unsaturated zone flow.

Figure 5 shows the effect of the parameter β_0 on the model predicted temporal response for δ=1. The effect is similar to that of the parameter θ. In the plots shown in the figure, the solid line represents the limiting case of unconfined aquifer flow without unsaturated zone flow. The results in the figure show clearly that the behavior predicted for the case of no unsaturated flow is significantly different from that accounting for unsaturated flow. The implication of this result is that parameters estimated with the model not accounting for unsaturated flow may be grossly in error for formations where such flow is significant.

The electrical conductivity of the confining unit relative to that of the saturated zone, namely $\sigma_{D,3}$, plays an important role in the magnitude of the SP signal measurable at land surface. Figure 6 shows this effect. Increasing values of $\sigma_{D,3}$ lead to decreasing signal strength at land surface, implying that an aquifer underlain with a clay unit (high electrical conductivity) would generate smaller signals at land surface than that underlain with a more resistive granite bedrock. This is because a more conductive confining unit would conduct the electric energy generated by electrokinetic coupling in the saturated zone downward and away from land surface. This is true for an unconfined aquifer overlain with an unsaturated zone with strong or weak electrokinetic coupling.

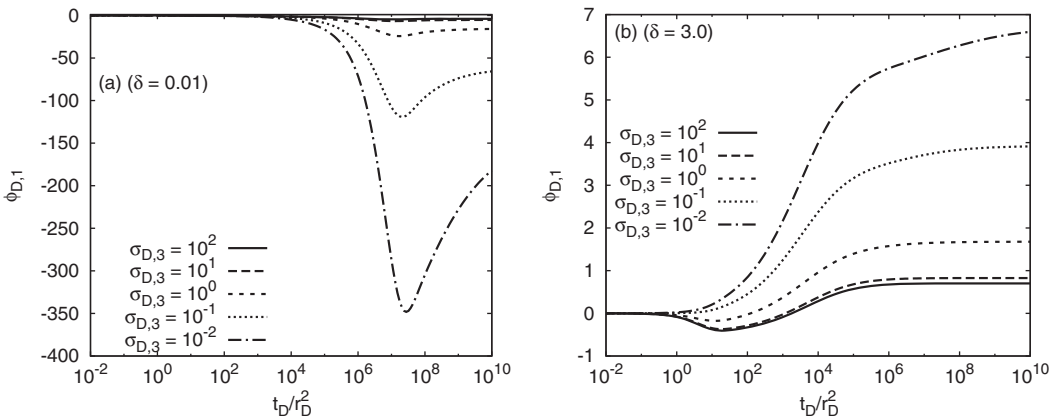

Figure 6. Dependence of model predicted SP at land surface on $\sigma_{D,3}$, the ratio of the confining unit electrical conductivity to that of the saturated zone.

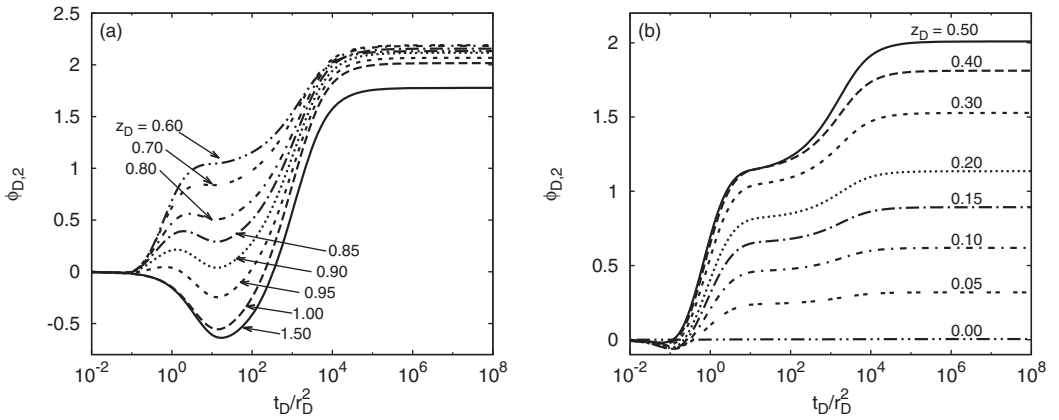

Figure 7. Temporal variation of model predicted SP response at different vertical positions, z_D, in the saturated zone. Plot shows responses (a) for $z_D > 0.5$ and (b) for $z_D \leq 0.5$.

5.2. Saturated Zone Response

It is intuitively clear that the measured SP signal should be larger in the saturated zone than at land surface. Hence, it is instructive to consider the model predicted behavior in the saturated zone. Figure 7 shows the saturated zone response at different vertical positions in the saturated zone for (a) $z_D > 0.5$ and (b) $z_D \leq 0.5$. The response at land surface, $z_D = 1.5$, is also included in (a) for comparison. For $z_D > 0.5$, the smallest signal is predicted at land surface. For cases with significant noise at land surface, it would be prudent to install electrodes at some depth closer to the water table. The results in the two plots also show a steady increase in signal strength upward from $z_D = 0$. Maximum response is predicted at some vertical position below, not at, the water table.

The effect of the dimensionless parameter δ of the SP response in the saturated zone is shown in Figure 8. As in the saturated zone response, varying the parameter δ leads to significant variation in model predicted behaviors. Figure 9 shows the effect of the parameter ϑ for (a) small and (b) large values of the parameter δ. Increasing values of ϑ shift the intermediate-time and late-time SP response to latter times as the water release due to unsaturated zone drainage relative to water release from elastic storage increases.

6. Comparison of Model Predicted Behavior to Lab-Scale Observations

In this section, lab-scale unconfined aquifer pumping tests are described. The SP responses are compared to model predicted behavior both qualitatively and quantitatively. Due to the complex and varied nature of the observed responses, only the saturated zone SP responses are used below to estimate hydraulic parameters. This is done despite the fact that SP data are typically collected at land surface. The parameter estimation exercise presented here is for proof-of-concept, demonstrating that the information content of saturated zone SP data is comparable to that of drawdown data. Future work will focus on detailed analysis of lab-scale and field-scale unsaturated zone responses.

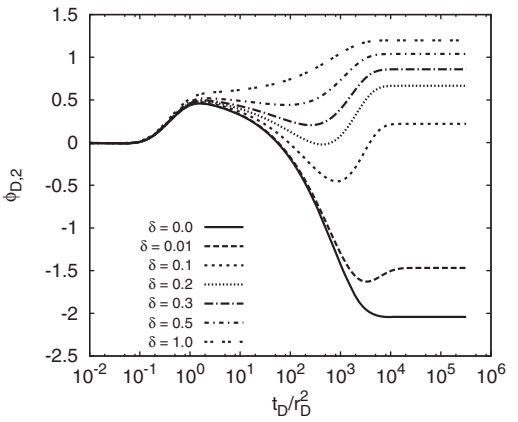

Figure 8. Model predicted SP response in the saturated zone at $z_D = 0.5$ for different values of the dimensionless parameter δ.

6.1. Experimental Setup and Materials

The experiments were performed in a finite cylindrical domain comprising two concentric cylinders of diameters 2.24 and 2.44 m. The surface of the inner cylinder was perforated, lined with a fine mesh, and filled with 40–70 98.2% silica sand to a depth of 85 cm. The sand tank was instrumented with 30 biomedical silver/silver chloride (Ag/AgCl)

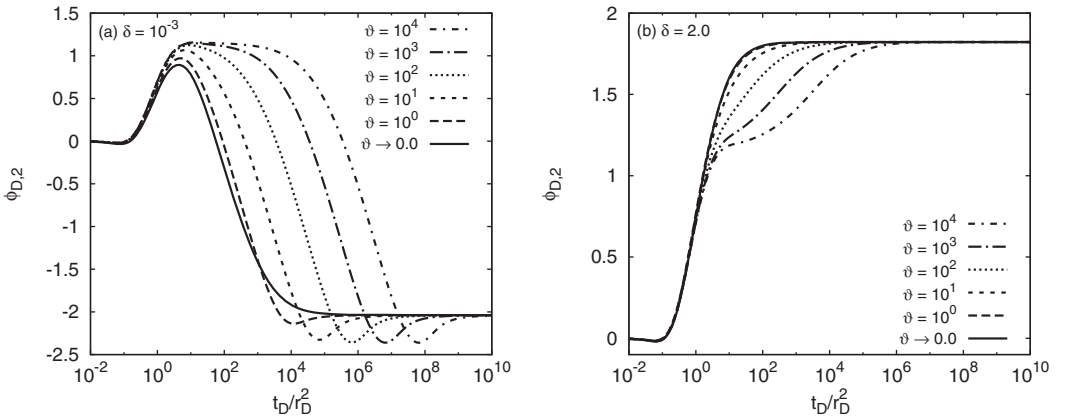

Figure 9. Temporal variation of model predicted saturated zone SP for different values of the dimensionless parameter ϑ with (a) $\delta=10^{-3}$ and (b) $\delta=2$.

electrodes and 6 lead/lead (II) chloride ($Pb/PbCl_2$) electrodes [*Petiau*, 2000], as well as with 3 piezometers and 10 soil moisture sensors (5tm Decagon Devices soil moisture probes). One reference electrode for each electrode type was placed in sand-filled polyvinyl chloride (PVC) tubes in the annulus (see Figure 10). An additional electrode of each type was placed in the annulus to monitor the annulus response to pumping. These electrodes were used to verify the validity of a Dirichlet SP boundary condition along the flow domain circumference in the same manner that the pressure transducer in the annulus was used to verify the flow boundary condition.

Deionized water was added to the sand tank until a nominal saturated thickness of 60 cm was achieved. Water in the annulus was used to maintain a constant head boundary along the flow domain circumference. The use of deionized water violates the assumption of negligible surface conductivity adopted in model development. This may lead to some unrealistic parameter values when the model developed above is applied to the data obtained in the experiments. It should be noted that the sand does contain some impurities that elevate the pore water ion concentrations to above those of deionized water [e.g., *Allègre et al*., 2010; *Jougnot and Linde*, 2013]. This was evidenced by the relatively high (compared to deionized water) pore water conductivity recorded during the experiments as discussed below.

A schematic of the experimental setup is shown in Figure 11. The biomedical electrodes (black dots in the schematic) were installed in sets of five at six different vertical positions $(z=\{5,30,55,60,65,70\}\text{cm})$ from the base of the sand tank. Along each radial line the electrodes were placed at $r=\{10,25,50,75,90\}$cm

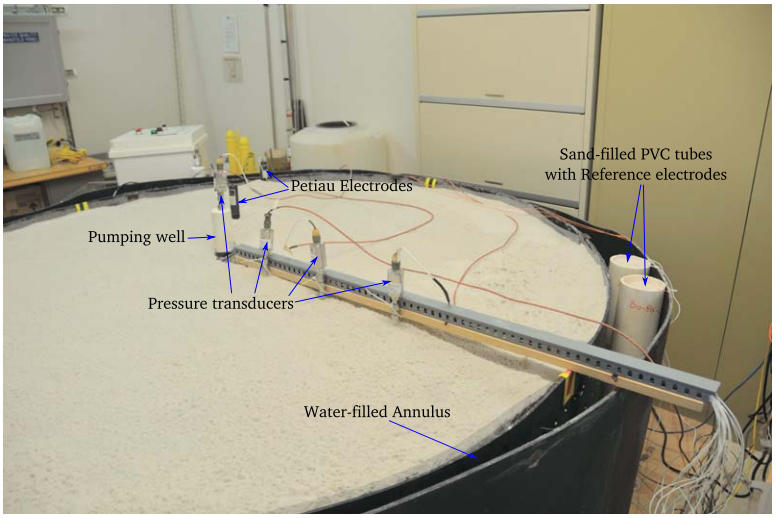

Figure 10. Lab-scale model used to conduct unconfined aquifer pumping tests.

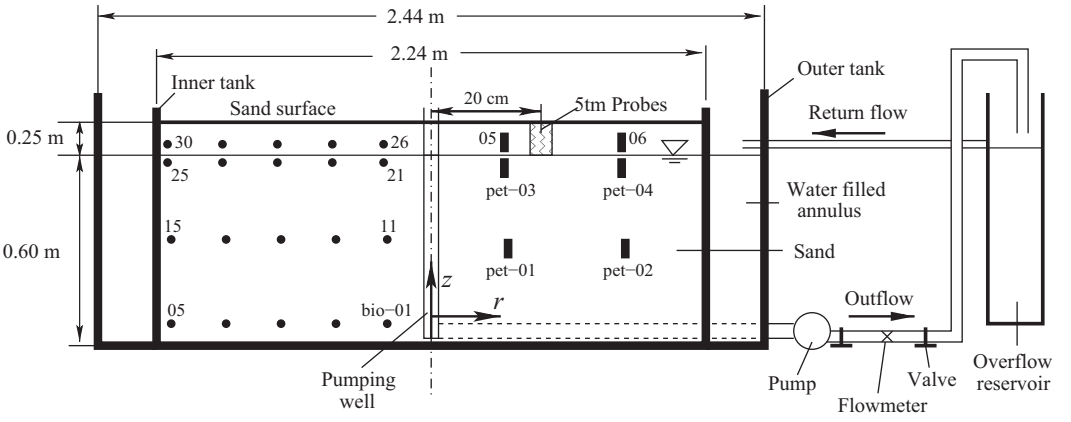

Figure 11. Schematic of the model showing sensor positions and sand tank dimensions.

from the axis of the tank. In Figure 11, they are numbered from the center outward, starting at the base of the sand tank, where electrodes bio-01–05 are the deepest, and bio-26–30 are closest to the surface. The electrodes bio-06–10 and bio-16–20 are not shown in the figure for clarity. Petiau electrodes are shown in the schematic as black rectangles and labeled pet-01–06. They were installed in three pairs at radii $r=\{25, 75\}$ cm and vertical positions $z=\{30, 55, 65\}$ cm.

The three piezometers were installed at $z = 30$ cm and at radii $r_1=25$, $r_2=50$, and $r_3=75$ cm. Pressure transducers were also placed in the pumping well $(r_w=2.54\text{cm})$ and the annulus. For the flow rates achievable in the experimental setup, only the pressure transducers in the pumping well and the piezometers closest to the well registered measurable pressure changes. Five soil moisture probes were installed along a radial profile at $z = 65$ cm, and five along a vertical profile at radial distance $r = 20$ cm from the center of the sand tank. Only the position of the vertical profile is highlighted in Figure 11, because the soil moisture data presented in this work are from these are probes. They are referred to here as 5tm-06–10, and were installed at depths $z'=\{5, 10, 12, 15, 20\}\text{cm}$ from the sand surface $(z'=85-z\text{cm})$.

During the pumping tests water was pumped from the sand tank via screened PVC tubing at the center of the flow domain into a fluid reservoir that was connected to the annulus between the two plastic cylinders by an overflow pipe. Pressure and flow rate data were collected every 5 s using Sixnet's VT-mIPm logger, while soil moisture data were collected every minute with a Campbell Scientific CR23X logger. SP data were collected with a Keithley 2701 logger, which serves as a high impedance (10 GΩ) voltmeter. Water discharged by the pump was routed through conductivity and pH meters for continuous monitoring before being circulated through the overflow reservoir. The conductivity of the annulus and overflow reservoir fluids was also monitored periodically during the course of a given test. After a prolonged period of equilibration following apparatus setup, effluent electrical conductivity stabilized at $\sigma_f \simeq 2.8\times10^{-2}\text{S/m}$. This is the value used in the analysis presented below for pore water conductivity. Annulus conductivity stabilized at a value of $8.7\times10^{-3}\text{S/m}$, indicating a concentration differential between the pore water and the annulus. In the analysis presented here, the potentials due to this differential in annulus and pore water conductivity are neglected.

6.2. Observed Behavior

Experiments were conducted in the apparatus discussed above at different flow rates and for different pumping phase durations. The pressure transducer in the annulus did not show appreciable pressure changes during the tests, validating the annulus as an effective constant head boundary. Example pumping test pressure and soil moisture data are shown in Figure 12. The pressure responses quickly attain a steady state, whereas the soil moisture responses show quasi-linear growth with time during the pumping phase. Both data show quick recovery after the pump is shut off, with soil moisture data showing significant residuals from pretest values. These residual responses are indicative of system hysteresis.

Example SP responses recorded during the pumping tests are shown in Figure 13 for a test with a pumping period of about 4 h. The graphs in (a) show data obtained at $z = 5$ cm with biomedical electrodes, which

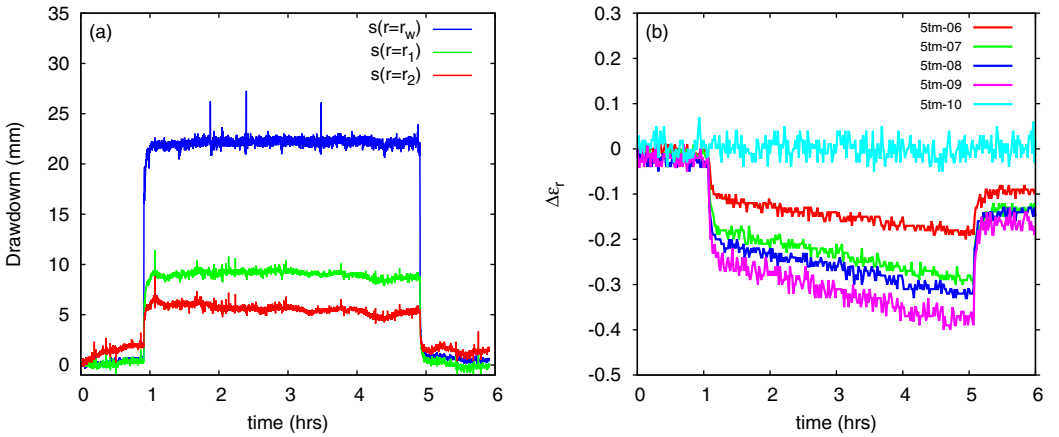

Figure 12. Plots of (a) drawdown and (b) soil moisture responses measured during a lab-scale pumping test. Soil moisture response is given in terms of $\Delta\varepsilon_r$, the change in relative dielectric permittivity. Here $r_w = 2.54$, $r_1 = 25$, and $r_2 = 50$ cm. Soil moisture data collected on vertical profile at $r = 20$ cm.

used below to estimate hydraulic parameters. Data obtained with all Petiau electrodes are shown in Figure 13b. The response (or lack thereof) of the electrodes in the annulus are included in the figures to show the validity of imposing a homogeneous Dirichlet boundary condition for SP along the flow domain circumference. Whereas the fluid pressure responses quickly reach a steady state, the SP response time scale is much longer, with the transient phase lasting for the entire duration of the pumping phase. The same can be said of the recovery phase, where both pressure and soil moisture transient responses proceed over a much shorter time scale than the SP recovery. The early time response is shown in Figure 14. These show a measurable *polarity* reversal predicted by the model developed above. This early time behavior was observed in measurements with both types of electrodes.

During the 4 h pumping test, the SP response did not achieve clear steady state. Therefore, a test with a longer (24 h) pumping phase was conducted. The results for electrodes bio-01–05 and bio-21–25 are shown in Figures 15a and 15b, while data from Petiau electrodes are in Figure 15c. The SP response does appear to attain a steady state after about 10 h of pumping. In addition, both biomedical and Petiau electrodes (bio-04, 23, 24, and 25 and pet-01) show some nonmonotonic behaviors, involving precipitous voltage drops followed by rapid rebound to a quasi-steady state. Such behavior is explainable by the model developed herein (see Figure 8).

In addition, one of the Petiau electrodes (pet-06) installed just above the water table shows some random perturbations (see Figures 15c and 15d) about the general transient response during both the pumping

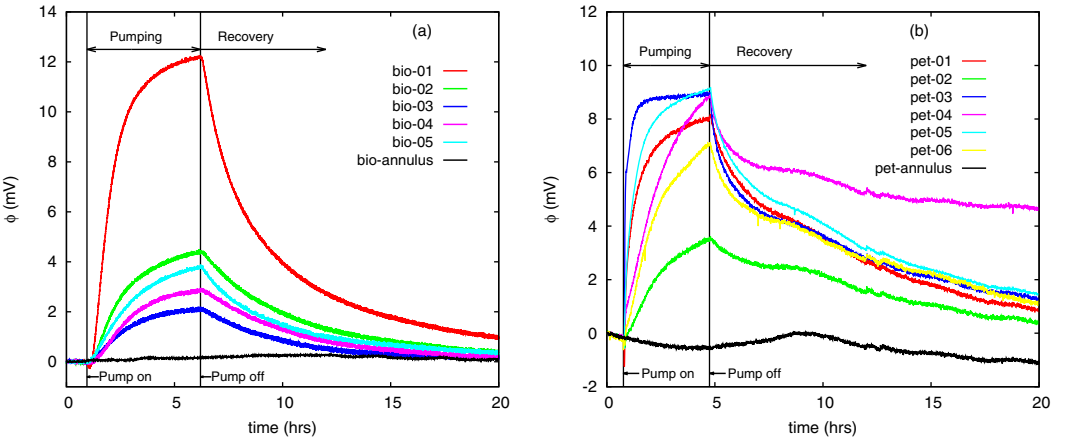

Figure 13. (a) Transient SP responses recorded during a ~2 day lab-scale pumping test using (a) biomedical (Ag/AgCl) and (b) Petiau ($Pb/PbCl_2$) electrodes.

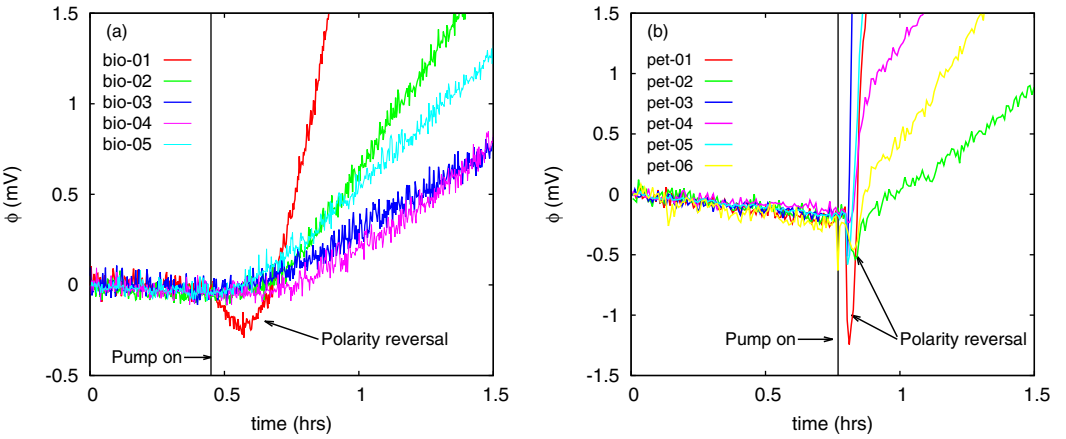

Figure 14. Close-up of the early time response recorded with (a) biomedical and (b) Petiau electrodes illustrating early time polarity reversal.

and recovery phases. Given that they are not observed in most electrode responses, they may be attributable to electrode malfunction. They may also be attributable to Haines jumps (electric field bursts) caused by a nonwetting fluid (air, in our case) displacing a wetting fluid (water) in a porous material during drainage and imbibition, a phenomenon observed in experiments conducted recently by *Haas and Revil* [2009]. However, the characteristic time scale of decay (1200 s) of the perturbations observed in the present

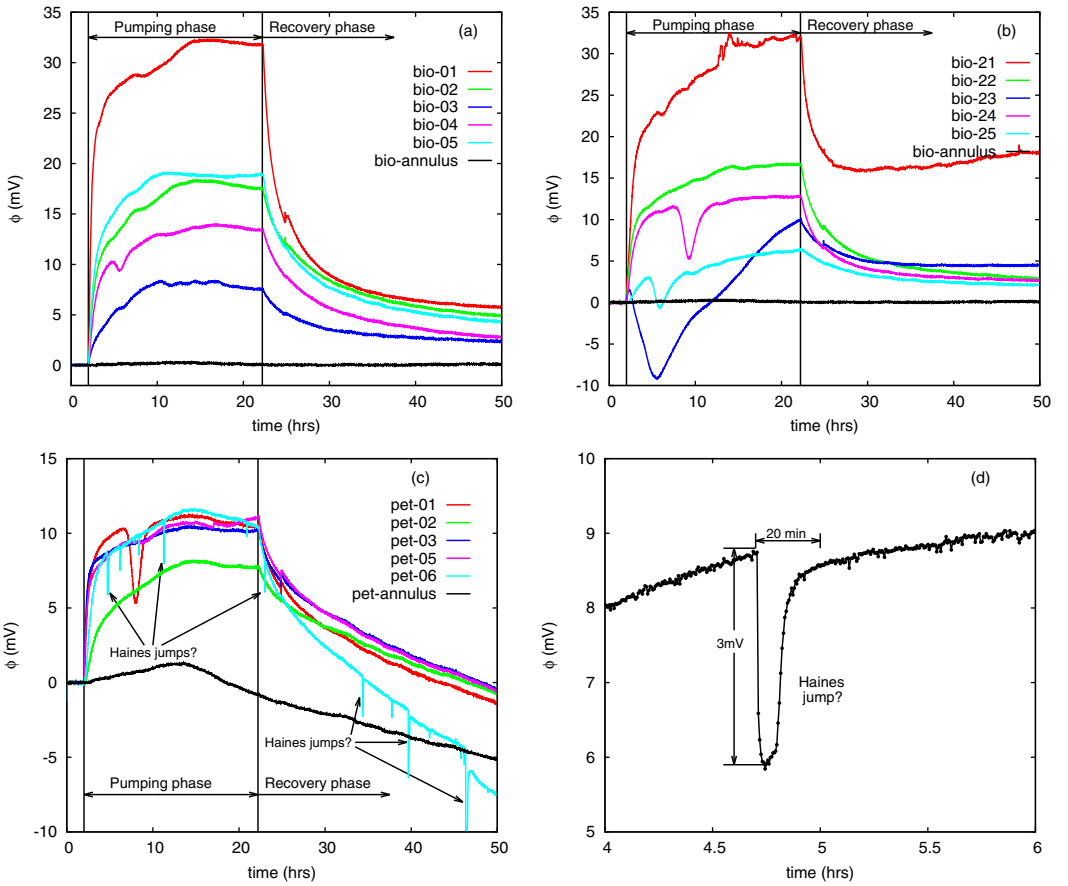

Figure 15. Transient SP responses recorded during a 2 day lab-scale pumping test using biomedical electrodes in the saturated zone (a) near the base and (b) near the water table, and (c) Petiau electrodes. (d) A close-up of a possible Haines jump observed just above the water table.

experiments are many orders-of-magnitude (4) larger than those observed by *Haas and Revil* [2009]. Whatever the mechanism of their generation, these perturbations are largely momentary and may be neglected (or filtered out) in analyses of the data.

6.3. Model Application to Data

The model developed above was used to estimate hydraulic parameters from drawdown and SP data collected in the experiments. Only pumping phase data were used in this analysis because system hysteresis associated with unsaturated zone drainage and imbibition during pumping and recovery is not accounted for in the model. System hysteresis implies that one set of unsaturated zone parameters may not be used to characterize both pumping and recovery phase system behavior. Drawdown data obtained in the pumping well and in the piezometer at $r = 25$ cm were used estimate hydraulic parameters K_r, κ, S_s, S_y, and β_0. Only SP data from electrodes bio-01, 02, and 03 are considered here. They are used to estimate the hydraulic parameters K_r, κ, S_s, S_y, and β_0, as well as the parameters δ and ℓ, which are associated only with the electric field problem.

Parameter estimation was performed with nonlinear least squares using the Marquardt-Levenberg algorithm as implemented in the MATLAB optimization toolkit. The flow domain in which the experiments were conducted is of finite radial extent. Linear superposition may be used to adapt the infinite domain solution developed above to the finite domain problem. However, the finite Hankel transform is the more computationally efficient approach [*Malama*, 2013]. When it is applied to the governing equations of flow and SP it yields the same solution in transform space as that already presented above. The difference between the finite and infinite transforms is simply the computation of the inverse, where one evaluates an infinite sum for the former, and an indefinite integral for the latter. For completeness, the definitions of the finite Hankel transform and its inverse are included in Appendix C. The finite inverse Hankel transform was used together with the method of *de Hoog et al*. [1982] for numerical inversion the solution from Hankel and Laplace space.

Parameter values estimated from drawdown and SP data are summarized in Table 2. The value of K_r estimated from drawdown data is comparable to the value of $K = 2.1 \times 10^{-4}$ m/s measured in falling-head permeameter experiments performed on the same sand (B. Malama and A. Revil, Estimation of hydraulic conductivity and electrokinetic coupling coefficient from streaming potentials measured in falling-head permeameter tests, submitted to *Ground Water*, 2013). The value of the specific yield also compares well to the measured porosity value of $n = 0.38$ for the sand when packed in a column (B. Malama and A. Revil, submitted manuscript, 2013). Estimates of K_r, S_y, and β_0 from SP data are close to those from drawdown data. It is clear that these parameters are sufficiently identifiable from SP data alone.

The value of the anisotropy ratio (κ) obtained from drawdown data is about half that estimated from SP data. Both estimates are greater than 1.0, indicating a higher vertical permeability. The specific storage (S_s) estimates differ significantly, with drawdown data yielding a larger value, but both estimates are much larger than is typically estimated from field-scale tests. This is because the model does not account for wellbore storage. It may also be due to large bulk medium compressibilities, which are attributable to (a) lack of cementation between the sand grains and (b) the low overburden stresses realizable in the lab-scale model. Specific storage comprises a fluid and medium compressibility, and may be expressed as

$$S_s = \rho g (n c_w + c_{bulk}), \psi \tag{54}$$

where c_w and c_{bulk} are water and bulk medium compressibilities, respectively. Using the average values of S_y from Table 2 for porosity and $c_w = 2.5 \times 10^{-10}$ Pa^{-1}, it follows that c_{bulk} 9.4×10^{-4} Pa^{-1} from drawdown, and

Table 2. Parameters Values Estimated From Drawdown and SP Data Collected in Lab-Scale Experiments.

Data	K_r ($\times 10^{-4}$ m/s)	κ (–)	S_s (m^{-1})	S_y (–)	β_0 (–)	δ ($\times 10^{-3}$) (–)	ℓ ($\times 10^{-9}$) (S·V/Pa·m))
$s(r = r_{D,w}) \leftarrow$	3.59	5.06	12.2	0.32	5.13	–	–
$s(r_D = 0.42) \leftarrow$	3.15	3.80	6.24	0.41	4.68	–	–
Average	3.37	4.43	9.22	0.37	4.91	–	–
bio-01	2.08	11.6	0.53	0.27	6.66	4.87	9.90
bio-02	3.61	9.76	1.00	0.31	5.64	5.68	3.70
bio-03	5.03	8.99	2.02	0.32	5.92	4.88	2.39
Average	3.57	10.1	1.18	0.30	6.07	5.14	5.33

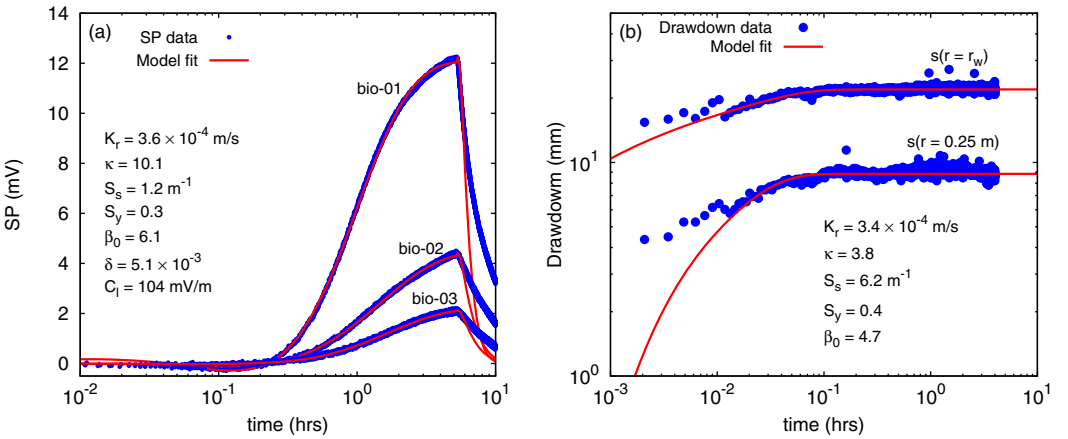

Figure 16. Model fits to (a) SP and (b) drawdown data collected in a lab-scale pumping test. Drawdown $s(r=r_w)$ was measured in the pumping well ($r_w=2.54$cm) while $s(r=25$ cm) was measured with a piezometer at $z = 30$ cm.

1.2×10^{-4}Pa^{-1} from SP data, respectively. These are large values compared to those typically estimated under field-scale test conditions. Reproducing field-scale values of c_{bulk} in a lab-scale model would require careful scaling and use of very low flow rates, which are not achievable in the model used for the current work.

In addition to the hydraulic parameters discussed above, SP data were used to estimate the parameters $\ell\psi$ and δ. The parameter $\ell\psi$ is used to calculate the electrokinetic coupling coefficient as $C_\ell=\gamma\ell/\sigma_2$ for the saturated zone, while δ measures the decay rate of the coupling coefficient with decreasing saturation in the unsaturated zone. The data yielded an average estimate of $C_{\ell\bar{\psi}}=-104$ mV/m, which compares well to the average value of -96 mV/m measured for the sand in falling-head permeameter experiments (B. Malama and A. Revil, submitted manuscript, 2013). The average estimate of $\delta \ll 1$, which indicates that the coupling coefficient decays at about the same rate as soil moisture with displacement above the water table.

Figure 16 shows the model fits to pumping phase SP data, and the predicted model behavior during recovery. The average values of the parameters estimated from the three data sets are also summarized in the figure. The model matches pumping phase data very well, but does not accurately predict recovery behavior. This mismatch between model and observed recovery behavior is attributable, in part, to hysteresis associated with drainage and imbibition. Unsaturated zone parameters (δ, β_0) estimated with pumping phase data cannot be used to predict recovery behavior.

7. Conclusion

A solution was developed for transient SP responses to radial flow toward a pumping well in an unconfined aquifer. The solution takes into account flow in the unsaturated zone using the approach of *Mishra and Neuman* [2010] where, for mathematical tractability, constitutive properties in the unsaturated zone are assumed to be exponential functions of matric potential (following *Gardner* [1958]). For the present work, adopting Archie's law leads to unsaturated zone electrical conductivity and electrokinetic coupling coefficient that are exponential functions of matric potential. Parameters for the unsaturated electrokinetic coupling coefficient are chosen such that it decays exponentially with increasing vertical position above the water table.

The resulting solution can be used to analyze transient SP data from unconfined aquifer tests where flow in the unsaturated zone is significant. In this work, the predicted response was compared both qualitatively and quantitatively to data collected in lab-scale unconfined aquifer tests. The model predicts, under certain parameter combinations, an early time *polarity* change in the SP response. Experimental data presented herein suggest that this polarity reversal is in fact observable at the lab scale. Additionally, nonmonotonic responses that do not yield polarity reversals (and are predicted by the model) were also observed in the experiments. Random SP fluctuations that could be due to Haines jumps or some other causal mechanism were detected just above the water table. Additional tests are required for more definitive evidence of the causal mechanism of these fluctuations, particularly because their temporal scales are many orders of magnitude larger than those associated with Haines jumps as observed by *Haas and Revil* [2009].

Though the primary focus of this work was development of a transient SP solution that accounts for unsaturated flow, the model was used to estimate hydraulic parameters from transient SP data. Parameters estimated in this manner show reasonable agreement with those from drawdown data. They also agree with those measured in falling-head permeameter tests reported by B. Malama and A. Revil (submitted manuscript, 2013). Unusually large values of the specific storage were obtained primarily due to a lack of cementation between the sand grains and the low overburden stresses. It is also possible that this may be due to the assumption of negligible surface conductivity, which is violated by use of deionized water in the experiments. We only analyzed saturated zone responses in this work. In field applications, SP data are typically collected at land surface. Hence future work is planned for a more exhaustive analysis of saturated and unsaturated zone SP data collected in lab-scale and field-scale experiments.

Appendix A: Flow Solution

In the following, $s_{D,i}=s_i/H_c$, where s_i is drawdown in layer i and $H_c=Q/(4\pi b_2 K_r)$. The hydraulic response in the unsaturated zone (with $a_c=a_k$) is governed by the dimensionless flow equation

$$\vartheta\psi\frac{\partial s_{D,1}}{\partial t_D}=\frac{1}{r_D}\frac{\partial\psi}{\partial r_D}\left(r_D\left(\frac{\partial s_{D,1}}{\partial r_D}\right)\right)+\kappa\frac{\partial^2 s_{D,1}}{\partial z_D^2}-\beta_0\kappa\frac{\partial s_{D,1}}{\partial z_D},\psi \tag{A1}$$

where $\vartheta=(\beta_0 S_y/S)e^{-\beta_0(\psi_{D,a}-\psi_{D,k})}$, $S=b_2S_s$, $\psi_{D,a}=\psi_a/b_2$, $\psi_{D,k}=\psi_k/b_2$, $t_D=t/T_c$, $r_D=r/b_2$, $z_D=z/b_2$, $\kappa=K_z/K_r$, $\beta_0=a_k b_2$. In this work, (A1) is solved subject to the initial and far-field boundary conditions

$$s_{D,1}(r_D,z_D,0)=\lim_{r_D\to\infty\leftarrow}s_{D,1}(r_D,z_D,t_D)\equiv 0,\psi \tag{A2}$$

and the homogeneous Neumann (symmetry) condition

$$\lim_{r_D\to 0}\left(r_D\left(\frac{\partial s_{D,1}}{\partial r_D}\right)\right)=0.\psi \tag{A3}$$

Additionally, drawdown and flux continuity conditions are applied at the water table.

Taking the Laplace and Hankel transforms of (A1) yields

$$\frac{\mathrm{d}^2 s_{D,1}}{\mathrm{d}z_D^2}-\beta_0\frac{\mathrm{d}s_{D,1}}{\mathrm{d}z_D}-\eta_1^2 s_{D,1}=0,\psi \tag{A4}$$

where $s_{D,1}$ is the Laplace and Hankel transform of s_D, $\eta_1^2=(p\vartheta+a^2)/\kappa$, a is the (dimensionless) Hankel transform parameter and p is the (dimensionless) Laplace transform parameter. To solve this problem, solutions of the form $s_{D,1}\quad e^{uz_D}$ are chosen, leading to the quadratic equation $u^2-\beta_0 u-\eta_1^2=0$. This quadratic equation has the solution $u=u_0(1\pm v)$, where $u_0=\beta_0/2$ and $v=\sqrt{1+(\eta_1/u_0)^2}$. Since $s_{D,1}$ has to be finite even as $z_D=b_{D,1}\to\infty$, only the root $u=u_0(1-v)$ is considered here. This requirement of $|s_{D,1}|<\psi\infty$ even as $z_D=b_{D,1}\to\infty$, is used here instead of applying the Neumann boundary condition at $z_D=b_{D,1}$ as in *Mishra and Neuman* [2010]. Hence, the general solution for matric potential response in the unsaturated zone is

$$s_{D,1}=A_0 e^{uz_D}, \tag{A5}$$

where A_0 is an integration constant to be determined from the boundary conditions for the saturated zone flow problem.

The saturated zone flow problem with the usual initial and boundary conditions has the general solution (in Laplace-Hankel transform space)

$$s_{D,2}=2A_{2,1}\cosh(\eta z_D)+\frac{2}{p\eta^2\kappa},\psi \tag{A6}$$

where $\eta^2=(p+a^2)/\kappa$ and $A_{2,1}$ is an integration constant. From the continuity condition for hydraulic head at the water table, namely $s_{D,2}|_{z_D=1}=s_{D,1}|_{z_D=1}$, it follows that

$$A_0 e^u = 2A_{2,1}\cosh(\eta) + \frac{2}{p\eta^2\kappa}.\psi \tag{A7}$$

From the flux continuity condition at the water table, viz, $s_{D,2}^{\prime\leftarrow}|_{z_D=1} = s_{D,1}^{\prime\leftarrow}|_{z_D=1}$, it follows that

$$uA_0 e^u = 2\eta A_{2,1}\sinh(\eta).\psi \tag{A8}$$

Solving equations (A7) and (A8) for A_0 and $A_{2,1}$ leads to

$$A_{2,1} = \frac{u}{p\eta^2\kappa\Delta_0},\psi \tag{A9}$$

and

$$A_0 = \frac{2e^{-u}}{p\eta\kappa\Delta_0}\sinh(\eta),\psi \tag{A10}$$

where $\Delta_0 = \eta\sinh(\eta) - u\cosh(\eta)$. Hence, the solution for unsaturated flow response, in Laplace-Hankel transform space is

$$s_{D,1} = \frac{2\sinh(\eta)}{p\eta\kappa\Delta_0}\overleftarrow{e^{u(z_D-1)}},\psi \tag{A11}$$

and that for the saturated zone is

$$s_{D,2} = \frac{2}{p(p+a^2)\leftarrow}1 + \frac{u}{\Delta_0}\cosh(\eta z_D)\leftrightarrow\psi \tag{A12}$$

This flow solution provides the primary forcing function in the SP problem, which is solved in Appendix B. This solution has a much simpler form than that obtained by *Mishra and Neuman* [2010] with a homogeneous Neumann (no flow) boundary condition at land surface. Since the flux at land surface may be nonzero due to evaporation, the solution developed above only satisfies the finiteness condition for the unsaturated zone.

Appendix B: SP Solution With Unsaturated Zone Flow

Taking Laplace and Hankel transforms of equation (31) and taking into account the initial condition and the far-field and symmetry boundary conditions, leads to

$$\frac{d^2\phi_{D,1}}{dz_D^2} - \beta_0 d\frac{d\phi_{D,1}}{dz_D} - a^2\phi_{D,1} = C_{\ell,r}F_1(a, z_D, p),\psi \tag{B1}$$

where

$$\begin{aligned} F_1(a, z_D, p) &= \frac{d^2 s_{D,1}}{dz_D^2} - \beta_1\frac{ds_{D,1}}{dz_D} - a^2 s_{D,1} \\ &= (u^2 - \beta_1 u - a^2)A_0 e^{uz_D},\psi \end{aligned} \tag{B2}$$

and $\beta_1 = -\partial\ln(\ell_\psi)/\partial z_D$. The relative electrokinetic coupling coefficient is

$$C_{\ell,r} = e^{-(\beta_1 - \beta_0 d)(z_D-1)}.\psi \tag{B3}$$

It follows then that

$$C_{\ell,r}F_1(a, z_D, p) = (u^2 - \beta_1 u - a^2)A_0 e^{(\beta_1 - \beta_0 d)}e^{(u-\beta_1+\beta_0 d)z_D}.\psi \tag{B4}$$

Hence, a particular solution that solves equation (B1) is

$$\phi_{D,p}(a,z_D,p)=B_0 e^{(u-\beta_1+\beta_0 d)z_D},\psi \tag{B5}$$

where B_0 is a constant of integration. Substituting (B5) into (B1), it can be shown that

$$B_0=\chi(a,p)A_0 e^{(\beta_1-\beta_0 d)},\psi \tag{B6}$$

which leads to the particular solution

$$\phi_{D,p}(a,z_D,p)=C_{\ell,r}(z_D)\chi(a,p)s_{D,1}(a,z_D,p),\psi \tag{B7}$$

where

$$\chi(a,p)=\frac{u^2-\beta_1 u-a^2}{(u-\beta_1+\beta_0 d)(u-\beta_1)-a^2}.\psi \tag{B8}$$

The homogeneous solution is obtained by solving

$$\frac{\mathrm{d}^2\phi_{D,1}^{*(0)\leftarrow}}{\mathrm{d}z_D^2}-\beta_0 d\frac{\mathrm{d}\phi_{D,1}^{*(0)\leftarrow}}{\mathrm{d}z_D}-a^2\phi_{D,1}^{*(0)\leftarrow}=0.\psi \tag{B9}$$

Considering solutions of the form $\phi_{D,1}^{*(0)\leftarrow}\ e^{xz_D}$, and then substituting into equation (B9) yields $x^2-\beta_0 dx-a^2=0$. This quadratic equation has the solutions $x=u_0 d(1\pm\hat{v})$ where $u_0=\beta_0/2$ and $\hat{v}=\sqrt{1+[a/(u_0 d)]^2}$. For $x=u_0 d(1+\hat{v})$, the solutions $\phi_{D,1}^{*(0)\leftarrow}\ e^{xz_D}$ grow with z_D and blow up as $z_D\rightarrow\infty$ (large z_D). Hence, we limit possible solutions to (B9) to those that satisfy $x=u_0 d(1-\hat{v})$. Hence, the set of homogeneous solutions considered here are

$$\phi_{D,1}^{(0)\leftarrow}=A_1 e^{-\hat{u}z_D}, \tag{B10}$$

where A_1 is an integration constant to be determined from continuity conditions at the water table, and $\hat{u}=u_0 d(\hat{v}-1)$.

Taking the Laplace and Hankel transforms of equation (31) for the saturated zone, and simplifying, one obtains

$$\frac{\mathrm{d}^2\phi_{D,2}}{\mathrm{d}z_D^2}-a^2\phi_{D,2}=(\eta^2-a^2)s_{D,2}-\frac{2}{p\kappa},\psi \tag{B11}$$

which has the general solution

$$\phi_{D,2}=\phi_{D,2}^{,(0)\leftarrow}+s_{D,2}(a,z_D,p),\psi \tag{B12}$$

where

$$\phi_{D,2}^{,(0)\leftarrow}=A_{2,1}e^{az_D}+A_{2,2}e^{-az_D}.\psi \tag{B13}$$

$A_{2,1}$ and $A_{2,2}$ are integration constants to be determined from boundary and continuity conditions.

Similarly, taking Laplace and Hankel transforms of equation (31) for the confining unit, leads to

$$\frac{\mathrm{d}^2\phi_{D,3}}{\mathrm{d}z_D^2}-a^2\phi_{D,3}=0,\psi \tag{B14}$$

which has the general solution

$$\phi_{D,3}=A_{3,1}e^{az_D}+A_{3,2}e^{-az_D}. \tag{B15}$$

For $\phi_{D,3}$ to be finite even as $z_D \rightarrow \leftarrow \infty$, $A_{3,1}$ must vanish identically, leading to

$$\phi_{D,3}=A_3 e^{az_D}, \tag{B16}$$

where we have set $A_{3,2}=A_3$. The four unknown constants A_1, $A_{2,1}$, $A_{2,2}$, and A_3 are determined from the four continuity conditions at the water table and at the base of the aquifer.

Applying the continuity of potential at the water table as given in equation (35) leads to

$$A_{2,1}e^{a}+A_{2,2}e^{-a}+s_{D,2}|_{z_D=1}=A_1 e^{-u_0 d(\hat{v}-1)}+\phi_{D,p}|_{z_D=1}.\psi \tag{B17}$$

Similarly, applying the potential gradient continuity condition given in equation (36) yields

$$aA_{2,1}e^{a}-aA_{2,2}e^{-a}+s'_{D,2}|_{z_D=1}=-u_0 d(\hat{v}-1)A_1 e^{-u_0 d(\hat{v}-1)}+\phi'_{D,p}|_{z_D=1}.\psi \tag{B18}$$

Eliminating A_1 from (B17) and (B18) leads to

$$X_{1,1}A_{2,1}+X_{1,2}A_{2,2}=Z_1,\psi \tag{B19}$$

where $X_{1,1}=(\hat{u}+a)e^{a}$, $X_{1,2}=(\hat{u}-a)e^{-a}$, $\hat{u}=u_0 d(\hat{v}-1)$, and

$$Z_1=\left(\hat{u}\phi_{D,p}+\phi'_{D,p}\right)|_{z_D=1}-\left(\hat{u}s_{D,2}+s'_{D,2}\right)|_{z_D=1}.\psi \tag{B20}$$

Applying the continuity conditions at the base of the aquifer gives

$$A_{2,1}+A_{2,2}-A_3=-s_{D,2}|_{z_D=0},\psi \tag{B21}$$

and

$$A_{2,1}-A_{2,2}-A_3\sigma_{D,3}=0.\psi \tag{B22}$$

Eliminating A_3 from these equations yields

$$X_{2,1}A_{2,1}+X_{2,2}A_{2,2}=Z_2,\psi \tag{B23}$$

where

$$X_{2,1}=\sigma_{D,3}-1,\psi \tag{B24}$$

$$X_{2,2}=\sigma_{D,3}+1,\psi \tag{B25}$$

and

$$Z_2=-\sigma_{D,3}s_{D,2}|_{z_D=0}.\psi \tag{B26}$$

Solving equations (B19) and (B23) yields

$$A_{2,1}=\frac{1}{2\Delta_1}\left(X_{2,2}Z_1-X_{1,2}Z_2\right),\psi \tag{B27}$$

and

$$A_{2,2}=\frac{1}{2\Delta_1}\left(X_{1,1}Z_2-X_{2,1}Z_1\right),\psi \tag{B28}$$

where

$$\Delta_1 = |(\hat{u}\sigma_{D,3}+a)\sinh(a)+(a\sigma_{D,3}+u)\cosh(a)|, \psi \quad \text{(B29)}$$

$$A_1 = e\hat{u}\ \ \phi_{D,2}-\phi_{D,p}\ \ |_{z_D=1}, \psi \quad \text{(B30)}$$

$$A_3 = \phi_{D,2}|_{z_D=0}, \psi \quad \text{(B31)}$$

$$\phi_{D,2}^{,(0)\leftarrow} = \frac{1}{\Delta_1}[Z_1 w_1(a,z_D) - Z_2 w_2(a,z_D)], \psi \quad \text{(B32)}$$

$$w_1(a,z_D) = \sigma_{D,3}\sinh(az_D)+\cosh(az_D), \psi \quad \text{(B33)}$$

and

$$w_2(a,z_D) = \hat{u}\sinh[a(z_D-1)] - a\cosh[a(z_D-1)]. \psi \quad \text{(B34)}$$

The resulting solution is summarized in equations (41–51).

Appendix C: Finite Hankel Transform

The finite Hankel transform and its inverse are defined by

$$f\ (a) = \int_0^R f(r)J_0(ar)r\mathrm{d}r, \psi \quad \text{(C1)}$$

and

$$f(r) = \frac{2}{R^2}\sum_{a_1}^{\infty\leftarrow} \frac{f\ (a)J_0(ar)^{\leftarrow}}{J_1^2(aR)^{\leftarrow}}, \psi \quad \text{(C2)}$$

respectively, where R is the radius of the flow domain. The sequence $a_1, a_2, \psi..\psi$ in the infinite sum in equation (C2) is determined by

$$J_0(aR) = 0, \psi \quad \text{(C3)}$$

with $(0 < \psi a_1 < \psi a_2 < \psi..)$.

Notation

K_r	Radial aquifer hydraulic conductivity [LT^{-1}].
K_z	Vertical aquifer hydraulic conductivity [LT^{-1}].
k_r	Relative unsaturated zone hydraulic conductivity [−].
S_s	Specific storage [L^{-1}].
S_y	Specific yield [−].
S_w	Soil water saturation [−].
θ	Volumetric soil moisture content [−].
$\alpha = K_r/S_s$	Aquifer hydraulic diffusivity [L^2T^{-1}].
b_i	Thickness of ith layer [L].
s_i	Drawdown in ith layer [L].
σ_i	Electrical conductivity of ith layer [SL^{-1}].
σ_r	Relative unsaturated zone electrical conductivity [−].
σ_w	Pore water electrical conductivity [SL^{-1}].
ϕ_i	SP response in ith layer [V].
ψ	Matric potential (suction head) [L].
Q	Pumping rate [L^3/T].
z	Vertical distance, measured from base of aquifer [L].
r	Radial distance from center of pumping well [L].
t	Time since onset of pumping [T].

$C_{\ell,i}$	Electrokinetic coupling coefficient of *i*th layer [VL^{-1}].
$C_{\ell,r}$	Relative unsaturated zone electrokinetic coupling coefficient [−].
m	Archie's cementation (first) exponent [−].
d	Archie's second exponent [−].
n	Porosity [−].
p	Laplace transform parameter [−].
a	Hankel transform parameter [−].

Acknowledgments
This research is funded by WIPP programs administered by the Office of Environmental Management (EM) of the U.S Department of Energy. Sandia National Laboratories is a multiprogram laboratory managed and operated by Sandia Corporation, a wholly owned subsidiary of Lockheed Martin Corporation, for the U.S. Department of Energy's National Nuclear Security Administration under contract DE-AC04–94AL85000. We also sincerely thank the two anonymous reviewers for their insightful critiques, comments, and suggestions for additional analyses.

References

Abramowitz, M., and I. A. Stegun (1972), *Handbook of Mathematical Functions With Formulas, Graphs, and Mathematical Tables*, Dover, New York.
Allègre, V., L. Jouniaux, F. Lehmann, and P. Sailhac (2010), Streaming potential dependence on water-content in fontainebleau sand, *Geophys. J. Int.*, *182*(3), 1248–1266.
Bogoslovsky, V. A., and A. A. Ogilvy (1973), Deformations of natural electric fields near drainage structures, *Geophys. Prospect.*, *21*(4), 716–723, doi:10.1111/j.1365-2478.1973.tb00053.x.
Chandler, R. (1981), Transient streaming potential measurements on fluid-saturated porous structures: An experimental verification of Biot's slow wave in the quasi-static limit, *J. Acoust. Soc. Am.*, *70*(1), 116–121.
Darnet, M., G. Marquis, and P. Sailhac (2003), Estimating aquifer hydraulic properties from inversion of surface streaming potential (SP) anomalies, *Geophys. Res. Lett.*, *30*(13), 1679, doi:10.1029/2003GL017631.
de Hoog, F. R., J. H. Knight, and A. N. Stokes (1982), An improved method for numerical inversion of Laplace transforms, *SIAM J. Sci. Stat. Comput.*, *3*(3), 357–366.
Doussan, C., J. Jouniaux, and J. L. Thony (2002), Variations of self-potential and unsaturated water flow with time in sandy loam and clay loam soils, *J. Hydrol.*, *267*, 173–185.
Friedman, S. P. (2005), Soil properties influencing apparent electrical conductivity: A review, *Comput. Electron. Agric.*, *46*, 45–70.
Gardner, W. R. (1958), Some steady state solutions of unsaturated moisture flow equations with application to evaporation from a water table, *Soil Sci.*, *85*, 228–232.
Guichet, X., L. Jouniaux, and J.-P. Pozzi (2003), Streaming potential of a sand column in partial saturation conditions, *J. Geophys. Res.*, *108*(B3), 2141, doi:10.1029/2001JB001517.
Haas, A., and A. Revil (2009), Electrical burst signature of pore-scale displacements, *Water Resour. Res.*, *45*, W10202, doi:10.1029/2009WR008160.
Ishido, T., and H. Mizutani (1981), Experimental and theoretical basis of electrokinetic phenomena in rock-water systems and its applications to geophysics, *J. Geophys. Res.*, *86*(B3), 1763–1775, doi:10.1029/JB086iB03p01763.
Jackson, M. D. (2010), Multiphase electrokinetic coupling: Insights into the impact of fluid and charge distribution at the pore scale from a bundle of capillary tubes model, *J. Geophys. Res.*, *115*, B07206, doi:10.1029/2009JB007092.
Jougnot, D., and N. Linde (2013), Self-potentials in partially saturated media: The importance of explicit modeling of electrode effects, *Vadose Zone J.*, *12*(2), 274–294, doi:10.2136/vzj2012.0169.
Jougnot, D., N. Linde, A. Revil, and C. Doussan (2012), Derivation of soil specific streaming potential electrical parameters from hydrodynamic characteristics of partially saturated soils, *Vadose Zone J.*, *11*(1), 259–273, doi:10.2136/vzj2011.0086.
Linde, N., D. Jougnot, A. Revil, S. Matthäi, T. Arora, D. Renard, and C. Doussan (2007), Streaming current generation in two-phase flow conditions, *Geophys. Res. Lett.*, *34*, L03306, doi:10.1029/2006GL028878.
Linde, N., J. Doetsch, D. Jougnot, O. Genoni, Y. Durst, B. J. Minsley, T. Vogt, N. Pasquale, and J. Luster (2011), Self-potential investigations of a gravel bar in a restored river corridor, *Hydrol. Earth Syst. Sci.*, *15*, 729–742.
Maineult, A., E. Strobach, and J. Renner (2008), Self-potential signals induced by periodic pumping tests, *J. Geophys. Res.*, *113*, B01203, doi:10.1029/2007JB005193.
Malama, B. (2011), Alternative linearization of water table kinematic condition for unconfined aquifer pumping test modeling and its implications for specific yield estimates, *J. Hydrol.*, *399*(3–4), 141-147, doi:10.1016/j.jhydrol.2011.11.007.
Malama, B. (2013), Measurement of streaming potentials generated during laboratory simulations of unconfined aquifer pumping tests, in *Advances in Hydrogeology*, pp. 127–157, Springer, New York.
Malama, B., K. L. Kuhlman, and A. Revil (2009a), Theory of transient streaming potentials associated with axial-symmetric flow in unconfined aquifers, *Geophys. J. Int.*, *179*(2), 990–1003, doi:10.1111/j.1365-246X.2009.04,336.x.
Malama, B., A. Revil, and K. L. Kuhlman (2009b), A semi-analytical solution for transient streaming potentials associated with confined aquifer pumping tests, *Geophys. J. Int.*, *176*(3), 1007–1016, doi:10.1111/j.1365-246X.2008.04,014.
Mboh, C. M., J. A. Huisman, E. Zimmermann, and H. Vereecken (2012), Coupled hydrogeophysical inversion of streaming potential signals for unsaturated soil hydraulic properties, *Vadose Zone J.*, *11*(2), 205–216, doi:10.2136/vzj2011.0115.
Mishra, P. K., and S. P. Neuman (2010), Improved forward and inverse analyses of saturated–unsaturated flow toward a well in a compressible unconfined aquifer, *Water Resour. Res.*, *46*, W07508, doi:10.1029/2009WR008899.
Moench, A. F. (1994), Specific yield as determined by type-curve analysis of aquifer-test data, *Ground Water*, *32*(6), 949–957.
Moench, A. F. (1995), Combining the Neuman and Boulton models for flow to a well in an unconfined aquifer, *Ground Water*, *33*(3), 378–384.
Moench, A. F., S. P. Garabedian, and D. R. LeBlanc (2001), Estimation of hydraulic parameters from an unconfined aquifer test conducted in a glacial outwash deposit, Cape Cod, Massachusetts, *U.S. Geol. Surv. Prof. Pap., 1629*, pp. 1–12.
Neuman, S. P. (1972), Theory of flow in unconfined aquifers considering delayed response of the water table, *Water Resour. Res.*, *8*(4), 1031–1045, doi:10.1029/WR008i004p01031.
Nwankwor, G. I., J. A. Cherry, and R. W. Gillham (1984), A comparative study of specific yield determinations for a shallow sand aquifer, *Ground Water*, *22*(6), 764–772, doi:10.1111/j.1745-6584.1984.tb01445.x.
Petiau, G. (2000), Second generation lead-lead chloride electrodes for geophysical applications, *Pure Appl. Geophys.*, *157*(3), 357–382, doi:10.1007/s000240050004.

Revil, A., and A. Cerepi (2004), Streaming potentials in two-phase flow conditions, *Geophys. Res. Lett.*, *31*, L11605, doi:10.1029/2004GL020140.
Revil, A., and H. Mahardika (2013), Coupled hydromechanical and electromagnetic disturbances in unsaturated porous materials, *Water Resour. Res.*, *49*, 744–766, doi:10.1002/wrcr.20092.
Revil, A., V. Naudet, J. Nouzaret, and M. Pessel (2003), Principles of electrography applied to self-potential electrokinetic sources and hydrogeological applications, *Water Resour. Res.*, *39*(5), 1114, doi:10.1029/2001WR000916.
Revil, A., V. Naudet, and J. D. Meunier (2004), The hydroelectric problem of porous rocks: Inversion of the position of the water table from self–potential data, *Geophys. J. Int.*, *159*, 435–444.
Revil, A., N. Linde, A. Cerepi, D. Jougnot, S. Matthäi, and S. Finsterle (2007), Electrokinetic coupling in unsaturated porous media, *J. Colloid Interface Sci.*, *313*(1), 315–327.
Revil, A., C. Gevaudan, N. Lu, and A. Maineult (2008), Hysteresis of the self-potential response associated with harmonic pumping tests, *Geophys. Res. Lett.*, *35*, L16402, doi:10.1029/2008GL035025.
Rizzo, E., B. Suski, and A. Revil (2004), Self-potential signals associated with pumping tests experiments, *J. Geophys. Res.*, *109*, B10203, doi:10.1029/2004/JB003049.
Sailhac, P., and G. Marquis (2001), Analytic potential for the forward and inverse modeling of SP anomalies caused by subsurface fluid flow, *Geophys. Res. Lett.*, *28*(9), 1851–1854, doi:10.1029/2000GL01245.
Shampine, L. (2008), Vectorized adaptive quadrature in matlab, *J. Comput. Appl. Math.*, *211*, 131–140.
Sill, W. R. (1983), Self-potential modeling from primary flows, *Geophysics*, *48*(1), 76–86, doi:10.1190/1.1441409.
Straface, S., E. Rizzo, and F. Chidichimo (2010), Estimation of hydraulic conductivity and water table map in a large-scale laboratory model by means of the self-potential method, *J. Geophys. Res.*, *115*, B06105, doi:10.1029/2009JB007053.
Straface, S., E. Rizzo, V. Gianpaolo, and F. Chidichimo (2011), Estimation of hydraulic conductivity in a large-scale laboratory model by means of the self-potential method, *Int. Water Technol. J.*, *1*(1), 22–34.
Suski, B., E. Rizzo, and A. Revil (2004), A sandbox experiment of self-potential signals associated with a pumping test, *Vadose Zone J.*, *3*(4), 1193–1199, doi:10.2114/3.4.1193.
Tartakovsky, G. D., and S. P. Neuman (2007), Three-dimensional saturated–unsaturated flow with axial symmetry to a partially penetrating well in a compressible unconfined aquifer, *Water Resour. Res.*, *43*, W01410, doi:10.1029/2006WR005153.
Titov, K., Y. Ilyin, P. Konosavski, and A. Levitski (2002), Electrokinetic spontaneous polarization in porous media: Petrophysics and numerical modeling, *J. Hydrol.*, *267*, 207–216.
Titov, K., A. Revil, P. Konasovsky, S. Straface, and S. Troisi (2005), Numerical modeling of self-potential signals associated with a pumping test experiment, *Geophys. J. Int.*, *162*, 641–650.
Vinogradov, J., and M. Jackson (2011), Multiphase streaming potential in sandstones saturated with gas/brine and oil/brine during drainage and imbibition, *Geophys. Res. Lett.*, *38*, L01301, doi:10.1029/2010GL045726.
Wieder, T. (1999), Algorithm 794: Numerical Hankel Transform by the Fortran Program HANKEL, *ACM Trans. Math. Software*, *25*(2), 240–250.